Manuscript bioRxiv preprint doi: https://doi.org/10.1101/333153; this version posted June 25, 2018. The copyright holder for this preprint (which was not certified by peer review) is the author/funder, who has granted bioRxiv a license to display the preprint in perpetuity. It is made available under aCC-BY-NC-ND 4.0 International license.
Click here to Download Manuscript Sharma et al 2018 bioRxiv final.pdf

Phosphatidylinositol 5 phosphate 4-kinase regulates plasma-membrane PIP_3 turnover and insulin sensitivity in *Drosophila.*

Sanjeev Sharma*, Swarna Mathre*^, Ramya Visvanathan*, Dhananjay Shinde* and Padinjat Raghu*%

*National Centre for Biological Sciences, TIFR-GKVK Campus, Bellary Road, Bangalore 560065, India.

^Manipal University, Madhav Nagar, Manipal 576104, Karnataka, India

%corresponding author

Tel: +91-80-23666102

E-mail: praghu@ncbs.res.in

bioRxiv preprint doi: https://doi.org/10.1101/333153; this version posted June 25, 2018. The copyright holder for this preprint (which was not certified by peer review) is the author/funder, who has granted bioRxiv a license to display the preprint in perpetuity. It is made available under aCC-BY-NC-ND 4.0 International license.

Abstract

Phosphatidylinositol-3,4,5-trisphosphate (PIP_3) generation at the plasma membrane is a key event during activation of receptor tyrosine kinases such as the insulin receptor and is critical for normal growth and metabolism. The lipid kinases and phosphatases regulating PIP_3 levels are described but mechanisms controlling their activity remain unclear. We report that in *Drosophila*, phosphatidylinositol 5 phosphate 4-kinase (PIP4K) function at the plasma membrane is required for normal PIP_3 levels during insulin receptor activation. Depletion of PIP4K increases PIP_3 levels and augments sensitivity to insulin through enhanced Class I phosphoinositide 3-kinase (PI3K) activity. Animals lacking PIP4K show enhanced insulin signalling dependent phenotypes *in vivo* and are resistant to the metabolic consequences of a high-sugar diet, highlighting the importance of PIP4K in normal metabolism and development. Thus, PIP4Ks are key regulators of receptor tyrosine kinase signalling with implications for growth factor dependent processes including tumour growth, T-cell activation and metabolism.

bioRxiv preprint doi: https://doi.org/10.1101/333153; this version posted June 25, 2018. The copyright holder for this preprint (which was not certified by peer review) is the author/funder, who has granted bioRxiv a license to display the preprint in perpetuity. It is made available under aCC-BY-NC-ND 4.0 International license.

Introduction

Lipid kinases that can phosphorylate selected positions on the inositol head group of phosphatidylinositol (PI), generate second messengers that regulate multiple processes in eukaryotic cells. The generation of phosphatidylinositol 3,4,5-trisphosphate (PIP_3) through the action of Class I PI3K following growth factor receptor (e.g Insulin receptor) stimulation, is a widespread signalling reaction [1] that regulates normal growth and development [2]. The role of Class I PI3K activation in response to insulin receptor signalling is evolutionarily conserved and has been widely studied in metazoan models such as the fly, worm and mammals [3]. Robust control of the levels and the dynamics of PIP_3 turnover is essential to maintain fidelity and sensitivity of information transfer during insulin signalling. This is achieved through a number of different molecular mechanisms. The Class I PI3K enzyme is a dimer of a catalytic subunit (p110) whose activity is inhibited under unstimulated conditions by the regulatory subunit (p85/50/55/60). Upstream receptor activation and subsequent binding to p-Tyr residues on the receptor and adaptor proteins relieves this inhibition. In addition, lipid phosphatases are also important in controlling PIP_3 levels at the plasma membrane. PTEN, a 3-phosphatase, hydrolyzes PIP_3 to produce $PI(4,5)P_2$ [4] while SHIP2 is a 5-phosphate that generates $PI(3,4)P_2$ from PIP_3 [5]. It is well documented that mutations in genes encoding any of these enzymes can be oncogenic or result in metabolic syndromes. Loss of function in PTEN or gain of function in Class I PI3K genes results in tumour development [6] while loss of SHIP2 results in altered insulin sensitivity in mammals [7,8]. Thus, the control of receptor-activated PIP_3 levels is vital to the regulation of events that direct cell growth and metabolism.

Class I PI3K enzymes utilize phosphatidylinositol 4,5-bisphosphate [$PI(4,5)P_2$] as substrate to generate PIP_3. In animal cells, the major route of $PI(4,5)P_2$ synthesis is the action of phosphatidylinositol 4 phosphate 5-kinase (PIP5K), enzymes that use phosphatidylinositol 4-phosphate (PI4P) as substrate and phosphorylate position 5 of the inositol headgroup [9]. More

bioRxiv preprint doi: https://doi.org/10.1101/333153; this version posted June 25, 2018. The copyright holder for this preprint (which was not certified by peer review) is the author/funder, who has granted bioRxiv a license to display the preprint in perpetuity. It is made available under aCC-BY-NC-ND 4.0 International license.

recently, Cantley and colleagues have described a distinct class of lipid kinases, the phosphatidylinositol 5 phosphate 4-kinases (PIP4K), enzymes that utilize phosphatidylinositol 5-phosphate (PI5P) as substrate and phosphorylate position 4 to generate $PI(4,5)P_2$ [10]. Loss of PIP4Ks does not result in a drop in the mass of total cellular $PI(4,5)P_2$ but the levels of its preferred substrate, PI5P are elevated [[11], reviewed in [12]]. In mammalian cells, three isoforms of PIP4Ks occur, viz. PIP4K2A, PIP4K2B and PIP4K2C. The phenotypes of mouse knockouts in each of these genes suggest a role for PIP4Ks in regulating receptor tyrosine kinase and PI3K signaling; deletion of PIP4K2A and PIP4K2B is able to slow tumor growth in p53-/- mice [13]; depletion of PIP4K2C results in excessive T-cell activation [14] and loss of PIP4K2B in mice results in hyper-responsiveness to insulin and a progressive loss of body weight in adults [15]. Previous studies have linked PIP4K2B to insulin and PI3K signalling. Overexpression of PIP4K2B in CHO-IR cells (expressing extremely low levels of endogenous PIP4K2B) results in reduced PIP_3 production following insulin stimulation [16]. Similarly, in U2OS cells, acute doxycycline-induced overexpression of PIP4K2A reduces AKT activation seen on insulin stimulation although changes in PIP_3 levels were not reported under these conditions [17]. By contrast, a recent study has reported that in immortalized B-cells that carry a deletion of PIP4K2A, there is a reduction in PIP_3 levels following insulin stimulation [18]. Thus, although there are multiple lines of evidence suggesting a link between PIP4K and Class I PI3K signaling during insulin stimulation, the impact of the PIP4K function on PIP_3 levels remains unresolved.

It has been reported that loss of the only PIP4K in *Drosophila* results in a larval growth deficit and developmental delay. These phenotypes were associated with an overall reduction in the levels of $pS6K^{T398}$ and $pAKT^{S505}$, both outputs of *m*echanistic *T*arget *O*f *R*apamycin (mTOR) signalling. The systemic growth defect in the dPIP4K mutants ($dPIP4K^{29}$) could be rescued by enhancing mTOR complex 1(TORC1) activity through pan-larval overexpression of its activator Rheb [11,19]. Since

bioRxiv preprint doi: https://doi.org/10.1101/333153; this version posted June 25, 2018. The copyright holder for this preprint (which was not certified by peer review) is the author/funder, who has granted bioRxiv a license to display the preprint in perpetuity. It is made available under aCC-BY-NC-ND 4.0 International license.

93 then it has also been shown in mice that PIP4K2C can regulate TORC1 -mediated signalling in
94 immune cells [14]. The loss of PIP4K2C was also shown to enhance TORC1 outputs in Tsc1/2
95 deficient MEFs during starvation [20]. mTOR signalling can transduce multiple developmental and
96 environmental cues including growth factor signalling, amino acid and cellular ATP levels into
97 growth responses [21]. However, the relationship between PIP4K function and its role in regulating
98 TORC1 activity and Class I PI3K signaling remains unclear.
99
100 During *Drosophila* development, larval stages are accompanied by a dramatic increase in body size.
101 Much of this growth occurs without increases in cell number but via an increase in cellular biomass
102 that occurs in polyploid larval tissues such as the salivary gland and fat body [22]. One major
103 mechanism that drives this form of larval growth is the ongoing insulin signalling; characterized by
104 the endocrine secretion of insulin-like peptides (dILPs) from insulin-producing cells (IPCs) in the
105 larval brain and their action on peripheral tissues through the single insulin receptor in flies [23].
106 Removal of insulin receptor (*dInR*) activity [24] or the insulin receptor substrate (*chico*) [25] results
107 in reduced growth and delayed development through multiple mechanisms. In flies, cell size in the
108 salivary glands can be tuned by enhancing cell-specific Class I PI3K-dependent PIP_3 production [26].
109 In this study, we use salivary glands and fat body cells of *Drosophila* larvae to study the effect of
110 dPIP4K on insulin receptor activated, Class I PI3K signalling. We find that in *Drosophila* larval
111 salivary gland cells, loss of *dPIP4K* enhanced the growth-promoting effects of overexpressing
112 components of the insulin signalling pathway. dPIP4K regulates the levels of PIP_3 and the intrinsic
113 sensitivity to insulin at the plasma membrane. Insulin signalling activity is regulated through
114 negative feedback from TORC1 in cells [27,28]. This TORC1 dependent reduction in insulin-
115 stimulated PIP_3 production is rendered ineffective in the absence of dPIP4K. Finally, we show that
116 these cellular changes in insulin signalling have consequences on circulating sugar metabolism in
117 larvae and also their susceptibility to insulin resistance on a high-sugar diet. Altogether, we

bioRxiv preprint doi: https://doi.org/10.1101/333153; this version posted June 25, 2018. The copyright holder for this preprint (which was not certified by peer review) is the author/funder, who has granted bioRxiv a license to display the preprint in perpetuity. It is made available under aCC-BY-NC-ND 4.0 International license.

118 demonstrate an important physiological role for dPIP4K as a negative regulator of Class I PI3K
119 signaling during insulin stimulation in *Drosophila in vivo*.
120
121 ## Results
122 ### dPIP4K genetically interacts with the insulin receptor signalling pathway
123 Salivary glands are endo-replicative organs in *Drosophila* larvae that are composed of large polarized
124 polyploid cells. Previously, we have demonstrated the use of this organ as a model to study changes
125 in cell size [11,26]. Prior studies on insulin receptor signalling (scheme depicted in Fig. 1A) have
126 revealed a role for this pathway in the autonomous control of both cell size and proliferation [23,25].
127 However, direct evidence for such regulation in salivary glands has not been demonstrated.
128 Therefore, as a proof of principle, we depleted *dInR* levels through RNA interference (RNAi)
129 selectively in the salivary glands of 3rd instar larvae using the driver *AB1*Gal4. As expected, this
130 resulted in a reduction of the average size of salivary gland cells without a change in the number of
131 cells (Fig. 1B, C and S1A). Likewise, overexpression of *dInR* (Fig. 1D(i) and S1B) and *chico* (Fig. 1E(i)
132 and S1D) selectively in the salivary glands also results in an increase in cell size. Thus, insulin
133 receptor signalling regulates cell size in the salivary gland.
134
135 We then compared the effect of overexpressing *dInR* in wild-type and *dPIP4K*^{29} cells. When *dInR*
136 was over-expressed in *dPIP4K*^{29} (*AB1>dInR; dPIP4K*^{29}), we also found an increase in salivary gland
137 cell size (Fig.1D(ii) and S1C); but the increase in cell size elicited was significantly greater than that
138 seen in wild-type cells (*AB1>dInR*) (Fig. 1G). Similar results were seen when comparing the effect of
139 *chico* overexpression in wild-type and *dPIP4K*^{29} cells; i.e. *chico* overexpression elicited a larger
140 increase in cell size in *dPIP4K*^{29} compared to wild-type (Fig. 1E(ii) and Fig. S1E).
141

bioRxiv preprint doi: https://doi.org/10.1101/333153; this version posted June 25, 2018. The copyright holder for this preprint (which was not certified by peer review) is the author/funder, who has granted bioRxiv a license to display the preprint in perpetuity. It is made available under aCC-BY-NC-ND 4.0 International license.

Further, in order to decipher how dPIP4K specifically interacted with the insulin signalling pathway we tested if constitutively activating a downstream step will abolish the differences between wild-type and *dPIP4K*^{29} cells. For this, we expressed a constitutively active form of Phosphoinositide-Dependent Kinase-1 (PDK1) (PDK1^{A467V}) which is normally activated by PIP_3 downstream of insulin receptor activation and regulates cell growth [29,30]. Expression of PDK1^{A467V} in salivary glands results in an increase in cell size (Fig. 1F(i) and S1F) and this was also seen when PDK1^{A467V} was expressed in *dPIP4K*^{29} (Fig. 1F(ii) and S1G). However, in contrast to *dInR* and *chico* manipulations, the effect of overexpressing PDK1^{A467V} resulted in an equivalent cell size increase in wild-type and *dPIP4K*^{29} (Fig. 1G). These findings suggest that in *Drosophila* larval cells dPIP4K modulates insulin receptor signalling at a step likely prior to PDK1 activation.

PIP_3 levels are elevated in dPIP4K depleted larval tissues

An essential early event in InR signal transduction is the activation of Class I PI3K leading to the production of PIP_3 at the plasma membrane [1]. Therefore, we measured PIP_3 levels at the plasma membrane by imaging salivary glands from wandering third instar larvae expressing a PIP_3-specific probe (GFP::PH-GRP1) [31]. We observed that under basal conditions, plasma membrane PIP_3 in *dPIP4K*^{29} showed a small but significant elevation compared to wild-type cells (Fig. 2A(i)and (ii)). Similar results were observed in experiments with fat body cells, i.e. PIP_3 levels in *dPIP4K*^{29} fat body cells were elevated compared to wild type (Fig. 2B(i) and (ii)).

During larval development in *Drosophila*, nutritional cues and other signals result in the release of *Drosophila* Insulin-like peptides (dILPs) [32] that bind to and activate dInR triggering Class I PI3K activation and PIP_3 production. The elevated PIP_3 levels observed in *dPIP4K*^{29} tissues could, therefore, result from (i) enhanced production and release of dILPs (ii) upregulation in insulin receptor levels (iii) increase in activity of insulin receptor or events downstream of receptor

bioRxiv preprint doi: https://doi.org/10.1101/333153; this version posted June 25, 2018. The copyright holder for this preprint (which was not certified by peer review) is the author/funder, who has granted bioRxiv a license to display the preprint in perpetuity. It is made available under aCC-BY-NC-ND 4.0 International license.

activation. To distinguish between these possibilities, we performed Q-PCR analysis to measure the levels of *dILP2, 3, 5* mRNAs [the levels of these are known to be transcriptionally regulated] [23]. We found that the transcript levels for these dILPs were not upregulated in *dPIP4K*^{29} compared to wildtype (Fig. 2C). Since these were not altered, we tested for enhanced dILP release, by measuring the levels of dILP2 within the neurosecretory insulin-producing cells (IPCs) from the brains of wandering third instar larvae. Immunoreactivity for dILP2 produced in IPCs is expected to be lower when more of it is released into the hemolymph. We found that the average intensity of dILP2 immunostaining in the IPCs was not lower in *dPIP4K*^{29} compared to controls; instead, it showed a small increase (Fig. 2E(i) and (ii)). Thus, we found no evidence of elevated production and release of dILPs in 3rd instar larvae that might explain the increased PIP_3 levels observed in *dPIP4K*^{29}. Further, we observed that *InR* receptor mRNA levels were also not different between *dPIP4K*^{29} and wildtype indicating that levels of InR that are activated by dILPs are also not likely to be different between the two genotypes (Fig. 2D). Collectively, our experiments show plasma membrane PIP_3 levels to be elevated in cells lacking dPIP4K without an increase in dILP secretion or cellular insulin receptor levels.

dPIP4K^{29} cells are intrinsically more sensitive to insulin stimulation.

We developed *ex-vivo* assays to test the sensitivity of larval tissues to bovine insulin. It has previously been shown that *Drosophila* cells respond to bovine insulin using signal transduction elements conserved with those proposed for the canonical mammalian insulin signalling pathway [33]. We observed that in salivary glands and fat body dissected from 3rd instar larvae, *ex-vivo* insulin stimulation triggered a rise in plasma membrane PIP_3 levels, measured using the GFP::PH-GRP1 probe. Interestingly, following insulin stimulation (10 min, 10 μM), the rise in PIP_3 levels in *dPIP4K*^{29} was higher than in wild type (Fig. 3A(i), A(ii)). Selective depletion of dPIP4K protein using RNAi specifically in the salivary gland cells also produced a similar result. (Fig. 3C(i) and (ii)). The

bioRxiv preprint doi: https://doi.org/10.1101/333153; this version posted June 25, 2018. The copyright holder for this preprint (which was not certified by peer review) is the author/funder, who has granted bioRxiv a license to display the preprint in perpetuity. It is made available under aCC-BY-NC-ND 4.0 International license.

192 increased sensitivity of *dPIP4K*^{29} cells to *ex-vivo* insulin stimulation could be reverted by specifically
193 reconstituting dPIP4K in salivary gland cells (Fig. 3D). Overexpression of dPIP4K in wild-type
194 salivary gland cells resulted in reduced levels of insulin-stimulated PIP_3 levels (Fig. 3E). A similar
195 observation was made in fat body cells dissected from larvae where PIP_3 production increased with
196 stimulation over a wide range (100-fold) of insulin concentrations used. While 100 nM of insulin
197 barely elicited an increase in plasma membrane PIP_3 levels, we observed that *dPIP4K*^{29} fat cells show
198 a larger rise in PIP_3 levels compared to the controls at higher concentrations (Fig. 3C(i)-(iii)).
199
200 **Quantitative measurements of PIP_3 mass in *Drosophila* larvae**
201 To test if the probe-based imaging of PIP_3 in single cells indeed reflects *in vivo* changes across the
202 animal, we refined and adapted existing protocols [34] to perform mass spectrometric
203 measurements of PIP_3 from *Drosophila* whole larval lipid extracts (Scheme depicted in Fig. 4A). The
204 amount of PIP_3 that has been detected and quantified from biological samples is in the range of a few
205 tens of picomoles [35]. We coupled liquid chromatography to high sensitivity mass spectrometry
206 (LCMS) and used a Multiple Reaction Monitoring (MRM) method to detect PIP_3 standards for
207 reliable quantification down to a few femtomoles (ca. 10 fmol, the lowest point in the figure inset on
208 the standard curve in Fig. S2(A). Since cellular lipids are composed of molecular species with varying
209 acyl chain lengths, we first characterized the PIP_3 species from *Drosophila* whole larval extracts
210 through use of neutral loss scans and thereafter quantified the abundance of these species. Fig. S2(B)
211 depicts the elution profiles of the different PIP_3 species that were reproducibly detected across
212 samples and Fig. S3(A) shows the relative abundance of various PIP_3 species. The 34:2 PIP_3 species
213 was found to be the most abundant. To standardize the procedure, we bisected whole larvae,
214 stimulated them with insulin and measured the levels of various PIP_3 species between samples with
215 and without insulin stimulation. Our LCMS method could clearly detect an increase in the levels of
216 several PIP_3 species upon insulin stimulation (Fig. S3(B)).

bioRxiv preprint doi: https://doi.org/10.1101/333153; this version posted June 25, 2018. The copyright holder for this preprint (which was not certified by peer review) is the author/funder, who has granted bioRxiv a license to display the preprint in perpetuity. It is made available under aCC-BY-NC-ND 4.0 International license.

Using this method, we compared PIP_3 levels from whole larval lipid extracts of various genotypes following insulin stimulation. We observed that compared to controls, *dPIP4K*^{29} larvae showed higher PIP_3 levels upon insulin stimulation (Fig. 4B(i), (ii)). Similarly, upon pan-larval knockdown of dPIP4K by RNAi enhanced PIP_3 levels were observed following insulin stimulation (Fig. S3C(ii) and (iii)) although the differences were not as striking as seen in *dPIP4K*^{29}; presumably this reflects the residual and variable amounts of dPIP4K protein seen during RNAi based knockdown ((Fig. S3C(i)). We also performed pan-larval rescue of dPIP4K protein in *dPIP4K*^{29} larvae and observed a trend of rescue in levels of various PIP_3 species (Fig. S3D(i) and (ii)). Finally, in an alternate setting, we also depleted dPIP4K in *Drosophila* S2 cells (inset in Fig. 4C(ii)) in culture using two independent dsRNA treatments and found that on insulin stimulation of serum starved cells, the total level of PIP_3 was enhanced compared to that in control cells (Fig. 4C(i)); the levels of individuals species of PIP_3 underlying this elevation broadly reflected those seen in experiments with *Drosophila* larval extracts (Fig. 4C(ii)). Together, the observations from these two independent assays (fluorescent probe based PIP_3 measurement and mass spectrometry) suggests that in dPIP4K depleted cells, increased amounts of PIP_3 are produced at the plasma membrane during insulin stimulation, thus implying that *dPIP4K* negatively regulates PIP_3 production.

dPIP4K directly regulates insulin receptor signalling independent of TORC1

We had previously reported a systemic reduction in TORC1 activity in *dPIP4K*^{29} larvae [11]. It is reported in mammalian cells that TORC1 activity can mediate feedback inhibition on insulin receptor substrate (IRS) to suppress insulin signalling and conversely reduced TORC1 activation can increase insulin signaling [28,36,37](Proposed feedback depicted in Fig.5 scheme 1 and 2) . We tested if the increased insulin-stimulated plasma membrane PIP_3 levels were a result of reduced cellular TORC1 activation in *dPIP4K*^{29}. We down-regulated Rheb, the GTPase that directly binds and activates TORC1 [38] in the salivary gland. *AB1>Rheb*^{RNAi} glands have substantially reduced cell

bioRxiv preprint doi: https://doi.org/10.1101/333153; this version posted June 25, 2018. The copyright holder for this preprint (which was not certified by peer review) is the author/funder, who has granted bioRxiv a license to display the preprint in perpetuity. It is made available under aCC-BY-NC-ND 4.0 International license.

size consistent with the known requirement for TORC1 signalling in regulating cell size (Fig. 5A (i)). Following insulin stimulation of *AB1>Rheb*^{RNAi} glands, PIP_3 levels at the plasma membrane were elevated compared to controls (Fig. 5A (ii)). Conversely, we compared PIP_3 production in control cells and those selectively overexpressing Rheb (*AB1>dRheb*) that is expected to enhance TORC1 activity. Following insulin stimulation, the levels of PIP_3 generated were significantly lower in *AB1>dRheb* glands compared to controls (Fig. 5B (i), (ii)). Similarly, knockdown of TSC, the GTPase activating protein (GAP) for Rheb, expected to result in hyperactivation of Rheb [39], also reduces the PIP_3 levels seen post insulin stimulation (Fig. 5C (i), (ii)). These results demonstrate that TORC1 output can control plasma membrane PIP_3 levels during insulin signaling in salivary gland cells (Fig.4 scheme 1 and 2).

We tested the effect of dPIP4K function on TORC1-mediated control of PIP_3 levels during insulin stimulation. When dPIP4K function is reconstituted in salivary glands (*AB1>dPIP4K; dPIP4K*^{29}), as expected, normal levels of insulin-stimulated PIP_3 production were restored (refer Fig. 3D). Knockdown of *dRheb* in *dPIP4K*^{29} salivary glands reduced the size of cells as expected (Fig. S5B(ii)) but also resulted in a further elevation of insulin-stimulated PIP_3 levels over that seen in *dPIP4K*^{29} (Fig. 5B(i), (ii)). However, when *dRheb* was overexpressed in *dPIP4K*^{29} salivary glands; (*AB1>dRheb; dPIP4K*^{29}), surprisingly, we found that insulin-stimulated PIP_3 levels were not lower than in *AB1>; dPIP4K*^{29} (Fig. 5D (i), (ii)). Likewise, depletion of TSC in *dPIP4K*^{29} (*AB1>Tsc*^{RNAi}*; dPIP4K*^{29}) did not lower insulin stimulated PIP_3 levels (Fig. 5F (i), (ii)). Thus, enhanced activation of TORC1 in salivary glands failed to complement the elevated PIP_3 levels resulting from loss of dPIP4K. Together, our findings indicate that dPIP4K function offers an additional mode of PIP_3 regulation that acts independent of TOR1 activity during insulin signalling.

bioRxiv preprint doi: https://doi.org/10.1101/333153; this version posted June 25, 2018. The copyright holder for this preprint (which was not certified by peer review) is the author/funder, who has granted bioRxiv a license to display the preprint in perpetuity. It is made available under aCC-BY-NC-ND 4.0 International license.

PIP4K is required at the plasma membrane to control of insulin-stimulated PIP_3 production

We and others have previously shown that PIP4Ks localize to multiple subcellular membrane compartments [11,40]. It is also reported that the substrate for this enzyme i.e. PI5P is present on various organellar membranes inside cells [41]. To further probe the mechanism of regulation of PIP_3 levels by dPIP4K, we decided to identify the sub-cellular compartment at which dPIP4K function is required to regulate PIP_3 levels. We generated transgenic flies to target dPIP4K to specific subcellular compartments (Fig. 6A). Using unique signal sequences, we targeted dPIP4K specifically to the plasma membrane (Fig. 6B (ii)), endomembrane compartments viz. the ER and Golgi (Fig. 6B (iii)) and the lysosomes (Fig. 6B (iv)). Lysates from S2R+ cells expressing these constructs for assayed for PIP4K activity and we found that all of the targeted dPIP4K enzymes were active (Fig. 6C(i)-(ii)); activity was proportional to the amount of protein expressed. Each of these targeted dPIP4K constructs were selectively reconstituted into dPIP4K null (*dPIP4K*^{29}) cells and tested for its ability to revert the enhanced insulin-stimulated PIP_3 production of *dPIP4K*^{29}. For this, we stimulated dissected salivary glands *ex-vivo* with insulin and measured PIP_3 production using the GFP::PH-GRP1 probe. Under these conditions, while endomembrane (Fig. 6E) and lysosome-targeted (Fig. 6F) dPIP4K failed to revert the elevated PIP_3 levels of *dPIP4K*^{29}, reconstitution with the plasma-membrane targeted dPIP4K completely restored the elevated PIP_3 levels in *dPIP4K*^{29} to that of controls (Fig. 6D). Further, overexpression of plasma-membrane targeted dPIP4K in wildtype salivary gland cells resulted in lower insulin stimulated PIP_3 levels compared to the controls at 5 mins post insulin stimulation (Fig. 6G). These observations suggest that plasma membrane localized dPIP4K is sufficient to regulate insulin-stimulated PIP_3 production.

We also tested the ability of plasma membrane localized PIP4K to regulate steps downstream of PIP3 production during insulin signalling. In a previous study, overexpression of human PIP4K2B in CHO-IR cells was shown to reduce the levels of $pAKT^{T308}$, an important PIP_3 dependent signalling

bioRxiv preprint doi: https://doi.org/10.1101/333153; this version posted June 25, 2018. The copyright holder for this preprint (which was not certified by peer review) is the author/funder, who has granted bioRxiv a license to display the preprint in perpetuity. It is made available under aCC-BY-NC-ND 4.0 International license.

event during insulin stimulation [16]. We tested the effect of overexpressing plasma membrane restricted PIP4K2B in these cells on $pAKT^{T308}$ during insulin stimulation. We generated a PIP4K2B construct with a CAAX-motif at its C-terminus (PIP4K2B::$mCherry^{CAAX}$) that localized the enzyme to the plasma membrane as expected, while the wildtype PIP4K2B (PIP4K2B::eGFP) can be seen at various subcellular compartments (Fig. 6H(i)). CHO-IR cells transiently overexpressing either PIP4K2B::eGFP or PIP4K2B::$mCherry^{CAAX}$ were serum starved, stimulated with insulin and $pAKT^{T308}$ was measured through immunoblotting. As previously reported, we found that PIP4K2B::eGFP overexpression resulted in a small but significant decrease in $pAKT^{T308}$ (Fig. 6H(ii)). Interestingly, consistent with our findings in *Drosophila* larval cells, we observed that over-expressed PIP4K2B::$mCherry^{CAAX}$ also caused a decrease in $pAKT^{T308}$. In fact, this decrease was achieved despite lower levels of expression of PIP4K2B::$mCherry^{CAAX}$ compared to the wildtype protein. Thus, PIP4K2B activity at the plasma membrane is sufficient to negatively regulate PIP_3 dependent $pAKT^{T308}$ levels in mammalian cells.

dPIP4K alters PIP_3 turnover by modifying Class I PI3K activity

PIP_3 levels at the plasma membrane upon insulin stimulation also depend on the length of time the receptor remains activated. Our 10-min stimulation protocol was based on earlier studies performed on *Drosophila* S2 cell-cultures where the response to insulin was maximal at 10 min [33]. However, in order to check for any differences in the dynamics of response to insulin, we also studied the time course of PIP_3 elevation following increasing times of insulin stimulation *ex-vivo*. Comparison of fixed preparations of salivary glands expressing GFP-PH-GRP1 probe showed a comparable time course of PIP_3 elevation but higher PIP_3 levels at every time point in $dPIP4K^{29}$ than in control glands (Fig. S4(i) and (ii)). To understand the effect of dPIP4K on insulin signaling at the plasma membrane with increased temporal resolution, we developed a live-imaging assay to follow the dynamics of PIP_3 turnover using the PH-GRP1 probe in salivary gland cells. A schematic of the reactions involved

bioRxiv preprint doi: https://doi.org/10.1101/333153; this version posted June 25, 2018. The copyright holder for this preprint (which was not certified by peer review) is the author/funder, who has granted bioRxiv a license to display the preprint in perpetuity. It is made available under aCC-BY-NC-ND 4.0 International license.

317 in the process and the assay protocol is depicted in Fig. 7A(i) and (ii). In this assay, during insulin
318 stimulation, the dynamics of PIP_3 turnover has three phases – (i) Rise phase – PIP_3 levels increase
319 after a stimulus owing to the activation of PI3K and relatively lower phosphatase activity (ii) Steady-
320 state phase – the opposing kinase and phosphatase activities regulating PIP_3 levels balance out each
321 other (iii) Decay phase - PI3K activity is irreversibly inhibited by wortmannin while PIP_3
322 phosphatases remain active. A single experimental trace is shown in Fig. 7B (i); insulin stimulation
323 triggers a rise in PIP_3 levels that peak and subsequently decline. Addition of wortmannin prior to
324 addition of insulin abolished insulin stimulated PIP_3 production establishing the effectiveness of
325 Class I PI3K inhibition in this assay (Fig. 7B(ii)). Under similar conditions, addition of the DMSO
326 vehicle post insulin did not reduce PIP_3 levels (Fig. 7B(iii)).
327
328 We tested the effect of loss of dPIP4K and tissue-specific overexpression of dPIP4K on PIP_3 turnover.
329 Loss of dPIP4K resulted in higher steady state levels of PIP_3 in salivary gland cells compared to
330 controls (Fig. 7C) while overexpression of dPIP4K resulted in lower steady-state levels of PIP_3 (Fig.
331 7D). These findings are consistent with the results from our imaging of PIP_3 levels from fixed salivary
332 glands of these genotypes (see Fig 3 A(ii) and E). We also analyzed the rate of change in PIP_3 levels
333 during the initial phase following insulin stimulation. This analysis clearly revealed an enhanced rate
334 of PIP_3 production on loss of *dPIP4K*[29] relative to controls and a reduced rate of PIP_3 production in
335 cells overexpressing this enzyme (Fig. 7E(i)). Thus, dPIP4K has the ability to modulate the rate of
336 PIP_3 production during insulin stimulation. A similar analysis of the rate of decrease in PIP_3 levels
337 during the phase after wortmannin addition (i.e when Class I PI3K activity has been inhibited)
338 showed a marginally slower rate of decay in PIP_3 levels in both dPIP4K depleted cells relative to
339 controls but also in cells overexpressing dPIP4K (Fig. 7E(ii)). This finding implies that while dPIP4K
340 function is able to modulate the PIP_3 phosphatase activity operative during insulin signalling in
341 *Drosophila* salivary gland cells, it has significantly greater effect on the Class I PI3K activity.

bioRxiv preprint doi: https://doi.org/10.1101/333153; this version posted June 25, 2018. The copyright holder for this preprint (which was not certified by peer review) is the author/funder, who has granted bioRxiv a license to display the preprint in perpetuity. It is made available under aCC-BY-NC-ND 4.0 International license.

342 ***dPIP4K* function regulates sugar metabolism during larval development.**

343 We tested if increased sensitivity to insulin seen in *dPIP4K*^{29} had any impact on the physiological
344 response of the animals to sugar intake. It has previously been reported that larvae raised on a high
345 sugar diet (HSD) develop an insulin resistance phenotypes reminiscent of Type II diabetes [42,43].
346 At the level of the organism, this includes reduced body weight, a developmental delay and elevated
347 levels of hemolymph trehalose, the main circulating sugar in insect hemolymph. As previously
348 reported, we found that when grown on HSD (1M sucrose), wild-type larvae show ca. 9 days delay
349 in development compared to animals grown on normal food (0.1M Sucrose) (Fig. 8A). However,
350 interestingly, in *dPIP4K*^{29} larvae grown on HSD a delay of only 5 days was seen compared to the
351 same genotype grown on 0.1M sucrose (Fig. 8A). We also biochemically measured the levels of
352 circulating trehalose in the hemolymph of wandering third instar larvae. It was observed that
353 *dPIP4K*^{29} larvae raised on normal food, showed circulating trehalose levels are *ca.* 40% lower
354 compared to controls. Further, when wild-type animals were grown on HSD, circulating trehalose
355 levels in larvae were elevated by ca. 25 % compared to that on normal food (Fig. 8B). However, when
356 *dPIP4K*^{29} larvae were raised on HSD, circulating trehalose levels remained essentially unchanged
357 (Fig. 8B) compared to that in animals grown on normal food. Together, these observations suggest
358 that increased insulin sensitivity occurring upon loss of dPIP4K confers partial protection against
359 phenotypes that arise when larvae are challenged with a high sugar diet.

360

361 ## Discussion

362 The generation of the signalling lipid PIP_3, is a conserved element of signal transduction by many
363 growth factor receptors. The enzymes that control PIP_3 levels during this process, namely Class I
364 PI3K and the lipid phosphatases PTEN and SHIP2 are well studied and the biological consequences
365 of mutations in genes encoding these enzymes underscore the importance of tight regulation of PIP_3
366 levels during growth factor signalling. While the roles of many of the core enzymes that are directly

bioRxiv preprint doi: https://doi.org/10.1101/333153; this version posted June 25, 2018. The copyright holder for this preprint (which was not certified by peer review) is the author/funder, who has granted bioRxiv a license to display the preprint in perpetuity. It is made available under aCC-BY-NC-ND 4.0 International license.

involved in PIP_3 metabolism have been studied extensively, the function of proteins that regulate their activity remains less understood; to date regulation of Class I PI3K activity by small GTPases (Ras, Rac) and $G_{\beta\gamma}$ subunits has been described [reviewed in [44]]. Although a role for PIP4K enzymes in regulating growth factor signalling through PIP_3 generation has been reported by earlier studies [15,16,18], the biochemical mechanism and cell-biological context in which they do so has remained obscure. PIP4Ks convert PI5P to $PI(4,5)P_2$ but to date no study has found a role for PIP4K in regulating overall cellular $PI(4,5)P_2$ levels [reviewed in [12]]. One possibility that has been raised is that PIP4Ks may generate the $PI(4,5)P_2$ pool from which PIP_3 is produced by Class I PI3K activity. Although PI5P, the preferred substrate of PIP4K, is a low abundance lipid, in principle, it is possible that a small, local pool of $PI(4,5)P_2$ is generated from PI5P by PIP4K and the loss of this small pool of $PI(4,5)P_2$ is not detected by the mass assays for estimating total cellular levels of this lipid. Quantitatively, based on their relative abundance, the small PIP4K generated pool of $PI(4,5)P_2$ is likely to be sufficient to serve as the substrate for PIP_3 generation by Class I PI3K. A recent study [18] has reported that PIP_3 levels are reduced in immortalized B-cells in which PIP4K2A activity is down regulated. By contrast, it has been previously reported that loss of PIP4K2B in mice results in increased levels of insulin signalling readouts such as $pAKT^{308}$ that are direct correlates of PIP_3 levels [15]. The exact reasons for these conflicting results is unclear and may include the different cell types used in each study; a key reason is likely to be the overlapping function of the three PIP4K isoforms present in mammalian genomes. In this study, we found that in *Drosophila*, that contains only a single gene encoding PIP4K activity (dPIP4K)[11,45], the levels of plasma membrane PIP_3 in cells lacking dPIP4K were elevated compared to controls. We established this finding using both a fluorescent reporter for plasma membrane PIP_3 in single cell assays using multiple cell types and also using lipid mass spectrometry across larval tissues and cultured, dPIP4K depleted *Drosophila* S2 cells. Thus, our study clearly demonstrates that in *Drosophila*, dPIP4K autonomously functions as a negative regulator of PIP_3 production during growth factor stimulation. The elevated PIP_3 levels seen

bioRxiv preprint doi: https://doi.org/10.1101/333153; this version posted June 25, 2018. The copyright holder for this preprint (which was not certified by peer review) is the author/funder, who has granted bioRxiv a license to display the preprint in perpetuity. It is made available under aCC-BY-NC-ND 4.0 International license.

when dPIP4K is depleted are not consistent with a role for this enzyme in generating the $PI(4,5)P_2$ at the plasma membrane used by Class I PI3K as substrate to generate PIP_3 during insulin signalling. Therefore, is likely that dPIP4K regulates PIP_3 levels through its ability to control the function of proteins that themselves regulate PIP_3 levels during Class I PI3K signalling.

In an earlier study [11], we had observed *dPIP4K*^{29} larvae have systemically reduced mTOR activation. In mammalian cells, reducing mTOR activity through the use of rapamycin or a loss of S6K, a direct target of TORC1, leads to increased activation of insulin signalling and obesity resistance associated with increased insulin sensitivity [46–48]. It is also reported that S6K inactivates IRS-1 by phosphorylating it on multiple serine residues [28,36]. Therefore, it is reasonable to hypothesize a scenario where the reduced TORC1 activity in *dPIP4K*^{29} cells may be the defect that drives the increase in the levels of PIP_3 in *dPIP4K*^{29}. In wild-type larval cells, modulating TORC1 activity had expected effects on cell size (Fig. S5A(i), B(i) and C(i)) but also could tune PIP_3 levels during insulin stimulation (Fig. 5A, C, E); enhancing TORC1 output resulted in lower levels of insulin-induced PIP_3 whereas reducing TORC1 activity caused higher levels of PIP_3. By contrast, overexpression of Rheb or the down-regulation of Tsc1/2 was not able to revert the elevated plasma membrane PIP_3 levels in *dPIP4K*^{29} cells (Fig. 5B, D and F) although they were able to restore the reduced cell size in *dPIP4K*^{29} (Fig. S5A(ii) and S5C(ii)). These results imply two conclusions: 1) Decreased TORC1 activity is not sufficient to explain the enhanced PIP_3 levels in *dPIP4K*^{29} larval cells and 2) Efficient feedback regulation of PIP_3 levels during receptor tyrosine kinase activation requires intact dPIP4K function in addition to TORC1 activity.

Binding of insulin to its receptor triggers a signalling cascade where the initial events occur at the plasma membrane. These involve interaction of the activated insulin receptor-ligand complex with IRS followed by the recruitment and activation of Class I PI3K at the plasma membrane. At which

bioRxiv preprint doi: https://doi.org/10.1101/333153; this version posted June 25, 2018. The copyright holder for this preprint (which was not certified by peer review) is the author/funder, who has granted bioRxiv a license to display the preprint in perpetuity. It is made available under aCC-BY-NC-ND 4.0 International license.

417 sub-cellular location is dPIP4K activity required to regulate this process? Fractionation and
418 immunolocalization studies in mammalian cells [40] and *Drosophila* [11] have indicated that PIP4K
419 isoforms are distributed across multiple subcellular compartments including the plasma membrane,
420 nucleus and internal vesicular compartments. In this study, using selective reconstitution of the
421 dPIP4K to specific membrane compartments, in cells devoid of any endogenous PIP4K protein, we
422 found that plasma membrane targeted dPIP4K could rescue the elevated PIP_3 levels in dPIP4K null
423 cells. This observation strongly suggests that the plasma membrane localized dPIP4K is sufficient to
424 control PIP_3 production during insulin stimulation. Our observation that *dPIP4K*^{29} cells were
425 hypersensitive to overexpression of *dINR* or *chico* compared to wild-type cells likely reflects the loss
426 of a dPIP4K dependent event in the control of PIP_3 levels at the plasma membrane. Overexpression
427 of plasma-membrane localized PIP4K2B was able to reduce $pAKT^{308}$ phosphorylation upon insulin
428 stimulation in mammalian cells just as well as the wildtype PIP4K2B enzyme. Our finding of a role
429 for the plasma membrane localized PIP4K in regulating PIP_3 levels in both *Drosophila* and
430 mammalian cells underscores the evolutionarily conserved nature of this mechanism. Previous
431 studies have shown that levels of PI5P, the substrate for PIP4Ks, increases upon insulin stimulation
432 and importantly, addition of exogenous PI5P can stimulate glucose uptake in a PI3K-dependent
433 manner [17,49]. Therefore, plasma membrane localized PIP4K and the levels of its substrate PI5P
434 could be a mechanism by which early events during insulin signalling are regulated.

435 What molecular event involved in PIP_3 turnover might dPIP4K regulate at the plasma membrane?
436 Using live cell imaging studies of PIP_3 turnover at the plasma membrane coupled with chemical
437 inhibition of Class I PI3K, we were able to observe that dPIP4K function has a substantial impact on
438 the rate of PIP_3 production following insulin stimulation whereas the rate of PIP_3 degradation was
439 only marginally affected. This finding suggests that dPIP4K likely regulates the activity of Class I
440 PI3K either directly or by controlling its coupling to the activated insulin receptor complex at the
441 plasma membrane; the exact mechanism by which it does so remains to be established.

bioRxiv preprint doi: https://doi.org/10.1101/333153; this version posted June 25, 2018. The copyright holder for this preprint (which was not certified by peer review) is the author/funder, who has granted bioRxiv a license to display the preprint in perpetuity. It is made available under aCC-BY-NC-ND 4.0 International license.

What might be the physiological consequence of losing dPIP4K mediated feedback control on PIP_3 production in the context of insulin signalling? Previous studies in mouse and human cells have reported that excessive activation of TORC1 signalling leads to inactivation of insulin signalling pathway and development of insulin resistance [50–52]. Since TORC1 activity is reduced [11] and PIP_3 were elevated (this study) in animals lacking dPIP4K, it is likely that loss of dPIP4K impacts sugar metabolism in *Drosophila* larvae. Using a recently reported high-sugar induced obesity and Type II diabetes-like disease model in *Drosophila* [42], we found that $dPIP4K^{29}$ larvae appear resistant to a high sugar diet as measured by the elevation in the hemolymph trehalose levels and they were relatively resistant to the developmental delay seen when wild-type larvae are reared on a high-sugar diet. This observation is reminiscent of that reported for the $PIP4K2B^{-/-}$ mice that have a reduced adult body weight compared to controls and clear blood glucose faster following a sugar bolus than control animals [15]. Our observation that dPIP4K at the plasma-membrane controls sensitivity to insulin receptor activation suggests a molecular basis for the physiological phenotypes observed in $dPIP4K^{29}$ larvae and $PIP4K2B^{-/-}$ mice. These observations also raise the possibility that inhibition of PIP4K activity may offer a route to reducing insulin resistance in the context of Type II diabetes. Such a mechanism may explain the hyperactivation of the T-cell receptor responses in mice lacking PIP4K2C [14], since the activation of Class I PI3K is a key element of T-cell receptor signal transduction. More generally, PIP4K activity likely offers a novel element of regulation for Class I PI3K activity in the context of receptor tyrosine kinase signalling.

bioRxiv preprint doi: https://doi.org/10.1101/333153; this version posted June 25, 2018. The copyright holder for this preprint (which was not certified by peer review) is the author/funder, who has granted bioRxiv a license to display the preprint in perpetuity. It is made available under aCC-BY-NC-ND 4.0 International license.

Materials and Methods

Drosophila strains and rearing –

Unless indicated, flies were grown on standard fly medium containing corn meal, yeast extract, sucrose, glucose, agar and antifungal agents. For all experiments, crosses were setup at 25°C in vials/bottles under non-crowded conditions.

Fly medium composition:

Ingredients	0.1 M sucrose	1 M sucrose
For 1 Litre		
Corn flour	80 g	80 g
D-Glucose	20 g	20 g
Sugar	40 g	342 g
Agar	8 g(4g)	8 g
Yeast powder	15 g	15 g
Propionic acid	4 ml	4 ml
TEGO(Methyl parahydroxy benzoate)	0.7 g	0.7 g
Orthophosphoric acid	0.6 ml	0.6 ml

The following stocks were used in the study: wildtype strain *Red Oregon R (ROR)*, *AB1-Gal4* (Bloomington # 1824), *UAS-dInR* (Bloomington # 8262), *UAS-Rheb*^{RNAi} (Bloomington TRiP # 33966), *UAS-Rheb* (Bloomington # 9688), *UAS-TSC*^{RNAi}(Bloomington TRiP # 52931), P{tGPH}4 (Bloomington # 8164), UAS-*dPIP4K*^{RNAi} (Bloomington TRiP # 65891). *UAS-dPIP4K::eGFP* and *dPIP4K*^{29} were generated in the lab and described in [11]. For PIP_3 measurements in the *dPIP4K*^{29} rescue experiment (Fig. 4F) using GFP-PH-GRP1 probe, we cloned dPIP4K cDNA (BDGP clone#

bioRxiv preprint doi: https://doi.org/10.1101/333153; this version posted June 25, 2018. The copyright holder for this preprint (which was not certified by peer review) is the author/funder, who has granted bioRxiv a license to display the preprint in perpetuity. It is made available under aCC-BY-NC-ND 4.0 International license.

LD10864) into pUAST-attB between *EcoRI* and *XhoI* sites without the GFP tag. The generation of flies expressing dPIP4K::-mCherry-CAAX is described in *Kumari K et.al, 2017*. For targeting dPIP4K to the endomembranes, the sequence QGSMGLPCVVM (*Sato.M et. al., 2006*) replaced the CAAX motif in the dPIP4K::mCherry-CAAX construct. To generate Lysosomal-dPIP4K::eGFP, the 39 amino-acid sequence from p18/LAMTOR (*Menon S et.al., 2014*) was used as a signal sequence. The signal sequence was commercially synthesized with a C-terminal flag tag and introduced upstream of dPIP4K::eGFP. The entire fusion construct was cloned into pUAST-attB by GIBSON assembly using *NotI* and *XbaI* sites. All molecular constructs conceptualized and analysed further with use of the molecular cloning tools available on the free online platform – Benchling.com. All transgenic lines were generated using insertions that were performed using site-specific recombination. The level of GFP fluorescence from lysosomal-dPIP4K::eGFP was observed to be very low in the salivary glands and did not interfere with our analysis PIP_3 measurements using the GFP-PH-GRP1 probe in Fig. 6F. All primer sequences used for cloning the different constructs are available on request.

Cell Culture, dsRNA treatment and Insulin stimulation assays –

CHO cell line stably expressing insulin receptor (isoform A) was a kind gift from Dr Nicholas Webster, UCSD. These were maintained at standard conditions in HF12 culture medium supplemented with 10% Fetal bovine serum and under G418 selection (400 µg/ml). Transfections were done 48 hrs. before the assay using FuGene, Promega Inc. as per manufacturer's protocols when the cultures were 50% confluent. For insulin stimulation assays, cells were starved overnight in HF12 medium without serum. Thereafter, the cells were de-adhered, collected into eppendorf tubes and stimulated with 1 µM insulin for indicated times. Post stimulation, cells were spun down and immediately lysed.

bioRxiv preprint doi: https://doi.org/10.1101/333153; this version posted June 25, 2018. The copyright holder for this preprint (which was not certified by peer review) is the author/funder, who has granted bioRxiv a license to display the preprint in perpetuity. It is made available under aCC-BY-NC-ND 4.0 International license.

S2R+ cells were cultured in Schneider's medium (GIBCO 21720024, HiMedia Labs IML003A) supplemented with 10% non-heat inactivated fetal bovine serum (US Origin, GIBCO 16000044) and contained antibiotics – streptomycin and penicillin (SIGMA G1146). dsRNA was synthesised in-house using Megascript RNAi Kit (Ambion, Life Technologies, AM1626) as per manufacturer's instructions. For dsRNA treatments, 0.5 X 10^6 cells were seeded into a 24-well plate. Once observed to be settled, cells were incubated with incomplete medium containing 1.875 µg of dsRNA. After 1 hour, an equal amount of complete medium was added to each well. The same procedure was repeated on each well 48 hours after initial transfection after removal of the spent medium from each well. Cells were harvested by trypsinization after a total of 96 hours of dsRNA treatment. For mass spectrometric estimation of PIP_3, S2R+ cells were pelleted down and stimulated with 1 µM insulin for 10 min. The reaction was stopped by the addition of ice-cold initial organic mix (described later in the section) and used for lipid extraction. The primer sequences used for dsRNA preparation are-

Ctrl (GFP)_dsRNA_Fwd	TAATACGACTCACTATAGGGATGGTGAGCAAGGGCGAGGAG
Ctrl (GFP)_dsRNA_Rev	TAATACGACTCACTATAGGGCTTGTACAGCTCGTCCATGCCG
PIP4K dsRNA I F (DRSC17213)	TAATACGACTCACTATAGGGAAGTTTGATTTAAAAGGTAGCAC
PIP4K dsRNA I R (DRSC17213)	TAATACGACTCACTATAGGGCTCAGCGTGTCCATTAGTTT
PIP4K dsRNA II F (DRSC39291)	TAATACGACTCACTATAGGGAAACATGCCGTCACATTTCA
PIP4K dsRNA II R (DRSC39291)	TAATACGACTCACTATAGGGGAGGTAACAGCGTTTTTCCG

Larval growth Curve Analysis -

Adult flies were made to lay eggs within a span of 4-6 hrs on normal food. After 24 hrs, newly hatched first instar larvae were collected and transferred in batches of about 15-25 larvae per into vials containing either 0.1/1M Sucrose in the fly media with other components unaltered. The vials were then observed to count the number of pupae.

bioRxiv preprint doi: https://doi.org/10.1101/333153; this version posted June 25, 2018. The copyright holder for this preprint (which was not certified by peer review) is the author/funder, who has granted bioRxiv a license to display the preprint in perpetuity. It is made available under aCC-BY-NC-ND 4.0 International license.

Hemolymph Trehalose Measurements –

The measurements were done exactly as described in [42]. In brief, hemolymph was pooled from five to eight larvae to obtain 1 µl for assay. The reagents used porcine trehalase (SIGMA, T8778) and GO kit (SIGMA, GAGO20)

Cell size analysis in salivary glands -

Salivary glands were dissected from wandering third instar larvae and fixed in 4% paraformaldehyde for 30 min at 4°C. Post fixation, glands were washed thrice with 1X PBS and incubated in BODIPY-FL-488 for 3 hours at room temperature. The glands were washed thrice in 1X PBS following which nuclei were labelled (using either DAPI or TOTO3) for 10 mins at room temperature and washed with 1X PBS again. The glands were then mounted in 70% glycerol and imaged within a day of mounting. Imaging was done on Olympus FV1000 Confocal LSM using a 20x objective. The images were then stitched into a 3D projection using an ImageJ plugin. These reconstituted 3D z-stacks were then analysed for nuclei numbers (correlate for cell number) and volume of the whole gland using Volocity Software (version 5.5.1, Perkin Elmer Inc.). The average cell size was calculated as the ratio of the average volume of the gland to the number of nuclei.

***Ex vivo* insulin stimulation and PIP_3 measurements in salivary glands and fat body** -

For experiments with salivary glands, wandering third instar larvae were dissected one larva at a time and glands were immediately dropped into a well of a 96-well plate containing either only PBS or PBS + 10 µM Insulin (75 µl) and incubated for 10 min at RT. Following this, 25 µl of 16% PFA was added into the same well to yield a final conc. of 4% PFA. The glands were fixed in this solution for 18 min at room temperature and then transferred sequentially to wells containing PBS every 10 min for 3 washes. Finally, glands were mounted in 80% glycerol in PBS containing antifade (0.4% propyl-gallate). For experiments with fat body lobes, late third instar feeding larvae were starved by placing

bioRxiv preprint doi: https://doi.org/10.1101/333153; this version posted June 25, 2018. The copyright holder for this preprint (which was not certified by peer review) is the author/funder, who has granted bioRxiv a license to display the preprint in perpetuity. It is made available under aCC-BY-NC-ND 4.0 International license.

547 them on a filter paper soaked in 1X PBS for 2 hrs. Thereafter, the incubation, fixation and mounting
548 steps were done exactly as described for salivary glands. Imaging was done on LSM 780 inverted
549 confocal microscope with a 20X/0.8 NA Plan Apochromat objective. For quantification, confocal
550 slices were manually curated to generate maximum z-projections of middle few planes of cells.
551 Thereafter, line profiles were drawn across clearly identifiable plasma membrane regions and their
552 adjacent cytosolic regions and ratios of mean intensities for these line profiles were calculated for
553 each cell. For salivary glands, about 10-15 cells from multiple glands were analysed and used to
554 generate statistics. For fat body, about 50 cells each from multiple animals were used for analysis.
555
556 For live imaging, salivary glands from wandering third instar larvae were dissected (glands from one
557 larva imaged in one imaging run) and placed inside a drop of imaging buffer (1X PBS containing
558 2mg/ml glucose) on a coverglass. The buffer was carefully and slowly soaked out with a paper tissue
559 to let the glands settle and adhere to the surface. Thereafter, the glands were immediately rehydrated
560 with 25 µl of imaging buffer. The imaging was done on Olympus FV3000 LSM confocal system using
561 a 10X objective. A total of 80 frames of a single plane were acquired, with 10s intervals. While
562 imaging, 25 µl of 20uM (2X) bovine insulin was used to stimulate the glands. After the steady state
563 was achieved, 50 µl of 800nM (2X) of wortmannin was added on top to inhibit PI3K activity.
564
565 **PIP_3 measurement by LC-MS/MS –**
566 The method was adopted and modified as required from [34].
567 **Lipid extraction –**
568 5 larvae were dissected in 1X PBS and transferred immediately into 37.5 µl of 1X PBS in a 2 ml
569 Eppendorf. For insulin stimulation, to this, 37.5 µl of 100 µM Insulin (final concentration – 50 µM)
570 was added and the tube was incubated on a mix mate shaker for 10 min at 500 rpm. At the end of
571 incubation time, 750 µl of ice-cold 2:1 MeOH:$CHCl_3$ organic mix was added to stop the reaction.

bioRxiv preprint doi: https://doi.org/10.1101/333153; this version posted June 25, 2018. The copyright holder for this preprint (which was not certified by peer review) is the author/funder, who has granted bioRxiv a license to display the preprint in perpetuity. It is made available under aCC-BY-NC-ND 4.0 International license.

572 Part of this solution was decanted and the rest of the mix containing larval tissues was transferred
573 into a homogenization tube. Larval tissues were homogenized in 4 cycles of 10 secs with 30 sec
574 intervals at 6000 rpm in a homogenizer (Precellys, Bertin Technologies). The tubes were kept on ice
575 at all intervals. The entire homogenate was then transferred to a fresh eppendorf and the
576 homogenization tube was then washed with the decanted mix kept aside earlier. 120 µl of water was
577 added to the homogenate collected in eppendorf, followed by addition of 5 ng of 17:0, 20:4 PIP_3
578 internal standard (ISD). The mixture was vortexed and 725 µl of chloroform was added to it. After
579 vortexing again for 2 min at around 1000-1500 rpm, the phases were separated by centrifugation for
580 3 min at 1500g. 1ml of lower organic phase was removed and stored in a fresh tube. To the remaining
581 aqueous upper phase, again 725 µl of chloroform was added. The mixture was vortexed and spun
582 down to separate the phases. Again, 1 ml of the organic phase was collected and pooled with the
583 previous collection (total of 2ml). This organic phase was used for measuring total organic
584 phosphate. To the aqueous phase, 500 µl of the initial organic mix was added followed by 170 µl of
585 2.4M HCl and 500 µl of $CHCl_3$. This mixture was vortexed for 5 min at 1000-1500 rpm and allowed
586 to stand at room temperature for 5 minutes. The phases were separated by centrifugation (1500g, 3
587 min). The lower organic phase was collected into a fresh tube by piercing through the protein band
588 sitting at the interface. To this, 708 µl of lower phase wash solution was added, the mixture was
589 vortexed and spun down (1500g, 3 min). The resultant lower organic phase was completely taken
590 out carefully into an Eppendorf tube and used for derivatization reaction.
591
592 **Extraction solvent mixtures:**
593 Initial organic mix: MeOH/Chloroform in the ratio of 484/242 ml, Lower Phase Wash Solution:
594 Methanol/1 M hydrochloric acid/ chloroform in a ratio of 235/245/15 ml. All ratios are expressed as
595 vol/vol/vol.
596

bioRxiv preprint doi: https://doi.org/10.1101/333153; this version posted June 25, 2018. The copyright holder for this preprint (which was not certified by peer review) is the author/funder, who has granted bioRxiv a license to display the preprint in perpetuity. It is made available under aCC-BY-NC-ND 4.0 International license.

Derivatization of Lipids –

To the organic phase of the sample, 50 µl of 2M TMS-Diazomethane was added (TO BE USED WITH ALL SAFETY PRECAUTIONS!). The reaction was allowed to proceed at room temperature for 10 min at 600 rpm. After 10 min, 10 µl of Glacial acetic acid was added to quench the reaction, vortexed briefly and spun down. 700 µl of post derivatization wash solvent was then added to the sample, vortexed (2 min, 1000-1500 rpm) and spun down. The upper aqueous phase was discarded and the wash step was repeated. To the final organic phase, 100 µl of 9:1 MeOH:H_2O mix was added and the sample was dried down to about 10-15 µl in a speedvac under vacuum.

Chromatographic separation and Mass spectrometric detection –

The larval lipid extracts were re-suspended in 170 µl LC-MS grade methanol and 30 µl LC-MS grade water. Samples were injected as duplicate runs of 3.5 µl. Chromatographic separation was performed on an Acquity UPLC BEH300 C4 column (100 x 1.0 mm; 1.7 µm particle size) purchased from Waters Corporation, USA on a Waters Aquity UPLC system and detected using an ABSCIEX 6500 QTRAP mass spectrometer. The flow rate was 100 µL/min. Gradients were run starting from 55% Buffer A (Water + 0.1% Formic Acid)- 45% Buffer B (Acetonitrile + 0.1% Formic acid) to 42% B from 0-5 min; thereafter 45% B to 100% B from 5-10 min; 100% B was held from 10-15 min; brought down from 100% B to 45% B between 15-16 min and held there till 20th min to re-equilibrate the column. On the mass spectrometer, in pilot standardization experiments, we first employed Neutral Loss Scans on biological samples to look for parent ions that would lose neutral fragments of 598 a.m.u indicative of PIP_3 lipid species (as described in [34]). Thereafter, these PIP_3 species were quantified in biological samples using the selective Multiple Reaction Monitoring (MRM) method in the positive mode. Only those MRM transitions that showed an increase upon insulin stimulation of biological samples were used for the final experiments (depicted in figure S3B). The MRM transitions for the different PIP_3 species quantified are listed out in the table below. Area of all the peaks was calculated on Sciex MultiQuant software. The area of the internal standard peak was used

bioRxiv preprint doi: https://doi.org/10.1101/333153; this version posted June 25, 2018. The copyright holder for this preprint (which was not certified by peer review) is the author/funder, who has granted bioRxiv a license to display the preprint in perpetuity. It is made available under aCC-BY-NC-ND 4.0 International license.

to normalize for lipid recovery during extraction. The normalized for each of the species was then divided by the amount of organic phosphate measured in each of the biological samples. The other mass spectrometer parameters are as follows: ESI voltage: +4500V; Dwell time: 40 ms ; DP (De-clustering Potential): 35.0 V; EP: (Entrance Potential): 10.1 V, CE (Collision Energy): 47.0 V; CXP (Collision cell Exit Potential): 11.6 V, Source Temperature : 450 C, Ion Spray Voltage – 4000 V, Curtain Gas : 35.0, GS1: 15, GS2: 16. The area under the peaks was extracted using MultiQuant v1.1 software (ABSCIEX). Numerical analysis was done in Microsoft Excel.

	Sample					
	Drosophila Larvae			S2R+ cells		
	PIP3 species	Parent Ion	Daughter Ion	PIP3 species	Parent Ion	Daughter Ion
MRM Transitions	32_1	1145.5	547.5	30_1	1119.5	521.5
	32_2	1177.5	579.5	32_0	1149.5	551.5
	34_1	1175.5	577.5	32_1	1147.5	549.5
	34_2	1173.5	575.5	32_2	1145.5	547.5
	34_3	1171.5	573.5	34_0	1177.5	579.5
	36_1	1203.5	605.5	34_1	1175.5	577.5
	36_2	1201.5	603.5	34_2	1173.5	575.5
	36_3	1199.5	601.5	34_3	1171.5	573.5
	36_4	1197.5	599.5	34_4	1169.5	571.5
				34_5	1167.5	569.5
				36_2	1201.5	603.5
				36_3	1199.5	601.5
				36_4	1197.5	599.5
				36_5	1195.5	597.5
				38_3	1227.5	629.5

bioRxiv preprint doi: https://doi.org/10.1101/333153; this version posted June 25, 2018. The copyright holder for this preprint (which was not certified by peer review) is the author/funder, who has granted bioRxiv a license to display the preprint in perpetuity. It is made available under aCC-BY-NC-ND 4.0 International license.

				38_4	1225.5	627.5
				38_5	1223.5	625.5
				37_4 ISD	1211.5	613.5

Total Organic Phosphate measurement–

1 ml of the organic phase from each sample was taken into phosphate-free tubes and dried completely at 90°C. The remaining steps were performed as described in *Thakur et.al., 2016.*

Preparation of S2R+ cell lysate for *in vitro* PI5P 4- kinase assay

The S2R+ cells were pelleted at 1000g for 10 min and washed with ice-cold PBS Twice. Cells were thereafter homogenized in lysis buffer containing 50mM Tris-Cl, pH – 7.5, 1mM EDTA, 1mM EGTA, 1% Triton-X-100, 50mM NaF, 0.27 M Sucrose, 0.1% β- Mercaptoethanol and freshly added protease and phosphatase inhibitors (Roche). The lysate was then centrifuged at 1000g for 15 min at 4 °C. Protein estimation was performed using the Bradford reagent according to the manufacturer's instructions.

PI5P4-kinase Assay

Vacuum-dried substrate lipid (6 µM PI5P) and 20 µM of phosphatidylserine were resuspended in 10 mM Tris pH 7.4 and micelles were formed by sonication for 2 min in a bath-sonicator. 50 µl of 2× PIPkinase reaction buffer (100 mM Tris pH 7.4, 20 mM $MgCl_2$, 140 mM KCl, and 2 mM EGTA) containing 20 µM ATP, 5 µCi [γ-^{32}P] ATP and cell lysates containing ~10 µg total protein was added to the micelles. The reaction mixture was incubated at 30 °C for 16 h. Lipids were extracted and resolved by one dimensional TLC (45:35:8:2 chloroform: methanol: water: 25% ammonia). The resolved lipids were imaged using phosphorImager.

bioRxiv preprint doi: https://doi.org/10.1101/333153; this version posted June 25, 2018. The copyright holder for this preprint (which was not certified by peer review) is the author/funder, who has granted bioRxiv a license to display the preprint in perpetuity. It is made available under aCC-BY-NC-ND 4.0 International license.

Western Blotting –

For larval western blots, lysates were prepared by homogenizing 3 wandering third instar larvae or 5 pairs of salivary glands from third instar larvae. In the case of CHO-IR cells, pelleted cells were lysed by repeated pipetting in lysis buffer (same as described above). Thereafter, the samples were heated at 95°C with Laemli loading buffer for 5 min and loaded onto an SDS- Polyacrylamide gel. The proteins were subsequently transferred onto a nitrocellulose membrane and incubated with indicated antibodies overnight at 4°C (for actin/tubulin incubation was done at room temperature for 3 hrs.). Primary antibody concentrations used were – anti- α-actin (SIGMA A5060) 1:1000; anti-dPIP4K 1:1000, anti – GAPDH (Novus Biologicals, #IM-5143A), anti-PIP4KB (Cell Signaling, #9694), anti – pAKTT308 (Cell Signaling, #9275), anti-AKT (Cell Signaling, # 9272). The blots were then washed thrice with Tris Buffer Saline containing 0.1% Tween-20 (0.1% TBS-T) and incubated with 1:10000 concentration of appropriate HRP-conjugated secondary antibodies (Jackson Laboratories, Inc.) for 1.5 hrs. After three washes with 0.1% TBS-T, blots were developed using Clarity Western ECL substrate on a GE ImageQuant LAS 4000 system.

Acknowledgements

This work was supported by the National Centre for Biological Sciences, TIFR, Department of Biotechnology, Ministry of Science and Technology (India); and a Wellcome Trust-DBT India Alliance Senior Fellowship to PR. S.S is a recipient of the S.P Mukherji Fellowship from CSIR and S.M an ICMR Fellowship. We thank the NCBS *Drosophila*, Imaging and Lipidomics Facility for support.

bioRxiv preprint doi: https://doi.org/10.1101/333153; this version posted June 25, 2018. The copyright holder for this preprint (which was not certified by peer review) is the author/funder, who has granted bioRxiv a license to display the preprint in perpetuity. It is made available under aCC-BY-NC-ND 4.0 International license.

676 ## References

677 1. Hawkins PT, Anderson KE, Davidson K, Stephens LR. Signalling through Class I PI3Ks in
678 mammalian cells. Biochem Soc Trans. 2006;34: 647–62. doi:10.1042/BST0340647
679 2. Engelman JA, Luo J, Cantley LC. The evolution of phosphatidylinositol 3-kinases as
680 regulators of growth and metabolism. 2006;7: 606–619. Available:
681 http://www.ncbi.nlm.nih.gov/entrez/query.fcgi?cmd=Retrieve&db=PubMed&dopt=Citatio
682 n&list_uids=16847462
683 3. Barbieri M, Bonafe M, Franceschi C, Paolisso G, Bonafè M, Franceschi C, et al. Insulin/IGF-
684 I-signaling pathway: an evolutionarily conserved mechanism of longevity from yeast to
685 humans. Am J Physiol Endocrinol Metab. 2003;285: 1064–1071.
686 doi:doi:10.1152/ajpendo.00296.2003
687 4. McConnachie G, Pass I, Walker SM, Downes CP. Interfacial kinetic analysis of the tumour
688 suppressor phosphatase, PTEN: evidence for activation by anionic phospholipids. Biochem
689 J. 2003;371: 947–955. doi:10.1042/bj20021848
690 5. Pesesse X, Moreau C, Drayer AL, Woscholski R, Parker P, Erneux C. The SH2 domain
691 containing inositol 5-phosphatase SHIP2 displays phosphatidylinositol 3,4,5-trisphosphate
692 and inositol 1,3,4,5-tetrakisphosphate 5-phosphatase activity. FEBS Lett. 1998;437: 301–303.
693 doi:10.1016/S0014-5793(98)01255-1
694 6. Luo J, Manning BD, Cantley LC. Targeting the PI3K-Akt pathway in human cancer: rationale
695 and promise. Cancer Cell. 2003;4: 257–62. Available:
696 http://www.ncbi.nlm.nih.gov/pubmed/14585353
697 7. Kaisaki PJ, Delépine M, Woon PY, Sebag-Montefiore L, Wilder SP, Menzel S, et al.
698 Polymorphisms in type II SH2 domain-containing inositol 5-phosphatase (INPPL1, SHIP2)
699 are associated with physiological abnormalities of the metabolic syndrome. Diabetes.
700 2004;53: 1900–4. Available: http://www.ncbi.nlm.nih.gov/pubmed/15220217

bioRxiv preprint doi: https://doi.org/10.1101/333153; this version posted June 25, 2018. The copyright holder for this preprint (which was not certified by peer review) is the author/funder, who has granted bioRxiv a license to display the preprint in perpetuity. It is made available under aCC-BY-NC-ND 4.0 International license.

8. Clément S, Krause U, Desmedt F, Tanti JF, Behrends J, Pesesse X, et al. The lipid phosphatase SHIP2 controls insulin sensitivity. Nature. 2001;409: 92–7. doi:10.1038/35051094

9. Stephens LR, Hughes KT, Irvine RF. Pathway of phosphatidylinositol(3,4,5)-trisphosphate synthesis in activated neutrophils. Nature. 1991;351: 33–9. doi:10.1038/351033a0

10. Rameh LE, Tolias KF, Duckworth BC, Cantley LC. A new pathway for synthesis of phosphatidylinositol-4,5-bisphosphate. Nature. 1997;390: 192–196.

11. Gupta A, Toscano S, Trivedi D, Jones DR, Mathre S, Clarke JH, et al. Phosphatidylinositol 5-phosphate 4-kinase (PIP4K) regulates TOR signaling and cell growth during Drosophila development. Proc Natl Acad Sci U S A. 2013;110: 5963–5968. doi:10.1073/pnas.1219333110

12. Kolay S, Basu U, Raghu P. Control of diverse subcellular processes by a single multi-functional lipid phosphatidylinositol 4,5-bisphosphate [PI(4,5)P2]. Biochem J. 2016;473: 1681–92. doi:10.1042/BCJ20160069

13. Emerling BM, Hurov JB, Poulogiannis G, Tsukazawa KS, Choo-Wing R, Wulf GM, et al. Depletion of a putatively druggable class of phosphatidylinositol kinases inhibits growth of p53-Null tumors. Cell. Elsevier; 2013;155: 844–857. doi:10.1016/j.cell.2013.09.057

14. Shim H, Wu C, Ramsamooj S, Bosch KN, Chen Z, Emerling BM, et al. Deletion of the gene *Pip4k2c* , a novel phosphatidylinositol kinase, results in hyperactivation of the immune system. Proc Natl Acad Sci. 2016;113: 7596–7601. doi:10.1073/pnas.1600934113

15. Lamia KA, Peroni OD, Kim YB, Rameh LE, Kahn BB, Cantley LC. Increased insulin sensitivity and reduced adiposity in phosphatidylinositol 5-phosphate 4-kinase beta-/- mice. Mol Cell Biol. 2004/05/15. 2004;24: 5080–5087. doi:10.1128/MCB.24.11.5080-5087.2004 24/11/5080 [pii]

16. Carricaburu V, Lamia KA, Lo E, Favereaux L, Payrastre B, Cantley LC, et al. The phosphatidylinositol (PI)-5-phosphate 4-kinase type II enzyme controls insulin signaling by regulating PI-3,4,5-trisphosphate degradation. Proc Natl Acad Sci. 2003;100: 9867–9872.

bioRxiv preprint doi: https://doi.org/10.1101/333153; this version posted June 25, 2018. The copyright holder for this preprint (which was not certified by peer review) is the author/funder, who has granted bioRxiv a license to display the preprint in perpetuity. It is made available under aCC-BY-NC-ND 4.0 International license.

doi:10.1073/pnas.1734038100

17. Jones DR, Foulger R, Keune W-J, Bultsma Y, Divecha N. PtdIns5P is an oxidative stress-induced second messenger that regulates PKB activation. FASEB J. 2013;27: 1644–56. doi:10.1096/fj.12-218842

18. Bulley SJ, Droubi A, Clarke JH, Anderson KE, Stephens LR, Hawkins PT, et al. In B cells, phosphatidylinositol 5-phosphate 4-kinase–α synthesizes $PI(4,5)P_2$ to impact mTORC2 and Akt signaling. Proc Natl Acad Sci. 2016;113: 10571–10576. doi:10.1073/pnas.1522478113

19. Durán R V, Hall MN. Regulation of TOR by small GTPases. EMBO Rep. 2012;13: 121–8. doi:10.1038/embor.2011.257

20. Mackey AM, Sarkes DA, Bettencourt I, Asara JM, Rameh LE. PIP4k is a substrate for mTORC1 that maintains basal mTORC1 signaling during starvation. Sci Signal. 2014;7: ra104-ra104. doi:10.1126/scisignal.2005191

21. Wullschleger S, Loewith R, Hall MN. TOR signaling in growth and metabolism. Cell. 2006;124: 471–84. doi:10.1016/j.cell.2006.01.016

22. Church RB, Robertson FW. Biochemical analysis of genetic differences in the growth of Drosophila. 1966/06/01. 1966;7: 383–407. Available: http://www.ncbi.nlm.nih.gov/entrez/query.fcgi?cmd=Retrieve&db=PubMed&dopt=Citation&list_uids=5940873

23. Brogiolo W, Stocker H, Ikeya T, Rintelen F, Fernandez R, Hafen E. An evolutionarily conserved function of the Drosophila insulin receptor and insulin-like peptides in growth control. Curr Biol. 2001;11: 213–21. Available: http://www.ncbi.nlm.nih.gov/pubmed/11250149

24. Shingleton AW, Das J, Vinicius L, Stern DL. The temporal requirements for insulin signaling during development in Drosophila. Johnston L, editor. PLoS Biol. 2005;3: e289. doi:10.1371/journal.pbio.0030289

bioRxiv preprint doi: https://doi.org/10.1101/333153; this version posted June 25, 2018. The copyright holder for this preprint (which was not certified by peer review) is the author/funder, who has granted bioRxiv a license to display the preprint in perpetuity. It is made available under aCC-BY-NC-ND 4.0 International license.

751 25. Bohni R, Riesgo-Escovar J, Oldham S, Brogiolo W, Stocker H, Andruss BF, et al. Autonomous
752 control of cell and organ size by CHICO, a Drosophila homolog of vertebrate IRS1-4.
753 1999;97: 865–875. Available:
754 http://www.ncbi.nlm.nih.gov/entrez/query.fcgi?cmd=Retrieve&db=PubMed&dopt=Citatio
755 n&list_uids=10399915
756 26. Georgiev P, Okkenhaug H, Drews A, Wright D, Lambert S, Flick M, et al. TRPM channels
757 mediate zinc homeostasis and cellular growth during Drosophila larval development. Cell
758 Metab. 2010;12: 386–97. doi:10.1016/j.cmet.2010.08.012
759 27. Kockel L, Kerr KS, Melnick M, Brückner K, Hebrok M, Perrimon N. Dynamic switch of
760 negative feedback regulation in Drosophila Akt-TOR signaling. PLoS Genet. 2010;6: 1–17.
761 doi:10.1371/journal.pgen.1000990
762 28. Gual P, Le Marchand-Brustel Y, Tanti J-F. Positive and negative regulation of insulin
763 signaling through IRS-1 phosphorylation. Biochimie. 2005;87: 99–109.
764 doi:10.1016/j.biochi.2004.10.019
765 29. Rintelen F, Stocker H, Thomas G, Hafen E. PDK1 regulates growth through Akt and S6K in
766 Drosophila. Proc Natl Acad Sci U S A. 2001;98: 15020–5. doi:10.1073/pnas.011318098
767 30. Paradis S, Ailion M, Toker A, Thomas JH, Ruvkun G. A PDK1 homolog is necessary and
768 sufficient to transduce AGE-1 PI3 kinase signals that regulate diapause in Caenorhabditis
769 elegans. Genes Dev. 1999;13: 1438–52. Available:
770 http://www.ncbi.nlm.nih.gov/pubmed/10364160
771 31. Britton JS, Lockwood WK, Li L, Cohen SM, Edgar BA. Drosophila's insulin/PI3-kinase
772 pathway coordinates cellular metabolism with nutritional conditions. 2002;2: 239–249.
773 Available:
774 http://www.ncbi.nlm.nih.gov/entrez/query.fcgi?cmd=Retrieve&db=PubMed&dopt=Citatio
775 n&list_uids=11832249

bioRxiv preprint doi: https://doi.org/10.1101/333153; this version posted June 25, 2018. The copyright holder for this preprint (which was not certified by peer review) is the author/funder, who has granted bioRxiv a license to display the preprint in perpetuity. It is made available under aCC-BY-NC-ND 4.0 International license.

776 32. Nässel DR, Broeck J Vanden. Insulin/IGF signaling in Drosophila and other insects: factors
777 that regulate production, release and post-release action of the insulin-like peptides. Cell Mol
778 Life Sci. 2016;73: 271–290. doi:10.1007/s00018-015-2063-3
779 33. Lizcano JM, Alrubaie S, Kieloch A, Deak M, Leevers SJ, Alessi DR. Insulin-induced
780 Drosophila S6 kinase activation requires phosphoinositide 3-kinase and protein kinase B.
781 Biochem J. 2003;374: 297–306. doi:10.1042/BJ20030577
782 34. Clark J, Anderson KE, Juvin V, Smith TS, Karpe F, Wakelam MJO, et al. Quantification of
783 PtdInsP3 molecular species in cells and tissues by mass spectrometry. Nat Methods. Nature
784 Publishing Group; 2011;8: 267–272. doi:10.1038/nmeth.1564
785 35. Malek M, Kielkowska A, Chessa T, Anderson KE, Barneda D, Pir P, et al. PTEN Regulates
786 PI(3,4)P2Signaling Downstream of Class I PI3K. Mol Cell. 2017;68: 566–580.e10.
787 doi:10.1016/j.molcel.2017.09.024
788 36. Tremblay F, Brûlé S, Hee Um S, Li Y, Masuda K, Roden M, et al. Identification of IRS-1 Ser-
789 1101 as a target of S6K1 in nutrient- and obesity-induced insulin resistance. Proc Natl Acad
790 Sci U S A. 2007;104: 14056–14061. doi:10.1073/pnas.0706517104
791 37. Zick Y. Insulin resistance: A phosphorylation-based uncoupling of insulin signaling. Trends
792 Cell Biol. 2001;11: 437–441. doi:10.1016/S0962-8924(01)02129-8
793 38. Tee AR, Manning BD, Roux PP, Cantley LC, Blenis J. Tuberous sclerosis complex gene
794 products, Tuberin and Hamartin, control mTOR signaling by acting as a GTPase-activating
795 protein complex toward Rheb. Curr Biol. 2003;13: 1259–68. Available:
796 http://www.ncbi.nlm.nih.gov/pubmed/12906785
797 39. Zhang Y, Gao X, Saucedo LJ, Ru B, Edgar B a, Pan D. Rheb is a direct target of the tuberous
798 sclerosis tumour suppressor proteins. Nat Cell Biol. 2003;5: 578–81. doi:10.1038/ncb999
799 40. Clarke JH, Wang M, Irvine RF. Localization, regulation and function of type II
800 phosphatidylinositol 5-phosphate 4-kinases. Adv Enzyme Regul. Elsevier Ltd; 2010;50: 12–

bioRxiv preprint doi: https://doi.org/10.1101/333153; this version posted June 25, 2018. The copyright holder for this preprint (which was not certified by peer review) is the author/funder, who has granted bioRxiv a license to display the preprint in perpetuity. It is made available under aCC-BY-NC-ND 4.0 International license.

18. doi:10.1016/j.advenzreg.2009.10.006

41. Sarkes D, Rameh LE. A novel HPLC-based approach makes possible the spatial characterization of cellular PtdIns5P and other phosphoinositides. Biochem J. 2010;428: 375–84. doi:10.1042/BJ20100129

42. Palanker Musselman L, Fink JL, Narzinski K, Ramachandran P V., Sukumar Hathiramani S, Cagan RL, et al. A high-sugar diet produces obesity and insulin resistance in wild-type Drosophila. Dis Model Mech. 2011;4: 842–849. doi:10.1242/dmm.007948

43. Pasco MY, Léopold P. High sugar-induced insulin resistance in Drosophila relies on the Lipocalin Neural Lazarillo. PLoS One. 2012;7: 1–8. doi:10.1371/journal.pone.0036583

44. Hawkins PT, Stephens LR. PI3K signalling in inflammation. Biochim Biophys Acta - Mol Cell Biol Lipids. 2015;1851: 882–897. doi:10.1016/j.bbalip.2014.12.006

45. Balakrishnan SS, Basu U, Raghu P. Phosphoinositide signalling in Drosophila. Biochim Biophys Acta - Mol Cell Biol Lipids. 2015;1851: 770–784. doi:10.1016/j.bbalip.2014.10.010

46. Reilly KEO, Rojo F, She Q, Solit D, Mills GB, Lane H, et al. mTOR Inhibition Induces Upstream Receptor Tyrosine Kinase Signaling and Activates Akt. Cancer Res. 2011;66: 1500–1508. doi:10.1158/0008-5472.CAN-05-2925.mTOR

47. Um SH, Frigerio F, Watanabe M, Picard F, Joaquin M, Sticker M, et al. Absence of S6K1 protects against age- and diet-induced obesity while enhancing insulin sensitivity. Nature. 2004;431: 200–205. doi:10.1038/nature02979

48. Haruta T, Uno T, Kawahara J, Takano A, Egawa K, Sharma PM, et al. A Rapamycin-Sensitive Pathway Down-Regulates Insulin Signaling via Phosphorylation and Proteasomal Degradation of Insulin Receptor Substrate-1. Mol Endocrinol. 2000; 783–794. doi:10.1210/mend.14.6.0446

49. Grainger DL, Tavelis C, Ryan AJ, Hinchliffe K a. Involvement of phosphatidylinositol 5-phosphate in insulin-stimulated glucose uptake in the L6 myotube model of skeletal muscle.

bioRxiv preprint doi: https://doi.org/10.1101/333153; this version posted June 25, 2018. The copyright holder for this preprint (which was not certified by peer review) is the author/funder, who has granted bioRxiv a license to display the preprint in perpetuity. It is made available under aCC-BY-NC-ND 4.0 International license.

Pflugers Arch. 2011;462: 723–32. doi:10.1007/s00424-011-1008-4

50. Harrington LS, Findlay GM, Gray A, Tolkacheva T, Wigfield S, Rebholz H, et al. The TSC1-2 tumor suppressor controls insulin-PI3K signaling via regulation of IRS proteins. J Cell Biol. 2004;166: 213–23. doi:10.1083/jcb.200403069

51. Shah OJ, Wang Z, Hunter T. Inappropriate Activation of the TSC/Rheb/mTOR/S6K Cassette Induces IRS1/2 Depletion, Insulin Resistance, and Cell Survival Deficiencies. Curr Biol. 2004;14: 1650–1656. doi:10.1016/j.cub.2004.08.026

52. Tzatsos A, Kandror K V. Nutrients suppress phosphatidylinositol 3-kinase/Akt signaling via raptor-dependent mTOR-mediated insulin receptor substrate 1 phosphorylation. Mol Cell Biol. 2006;26: 63–76. doi:10.1128/MCB.26.1.63-76.2006

bioRxiv preprint doi: https://doi.org/10.1101/333153; this version posted June 25, 2018. The copyright holder for this preprint (which was not certified by peer review) is the author/funder, who has granted bioRxiv a license to display the preprint in perpetuity. It is made available under aCC-BY-NC-ND 4.0 International license.

847 ## Figure Legends:

848 **Fig. 1. dPIP4K epistatically interacts with insulin receptor signalling to modulate cell size**

849 **A.** Schematic depicting the components of insulin signalling cascade studied in the subsequent
850 experiments. **B-G.** Salivary gland cell size measurements. **B.** Cell sizes upon knockdown of Insulin
851 receptor in salivary glands. **C.** Quantification of the no. of nuclei. Whiskers in the box plots represent
852 minimum and maximum values, with a line at the median. Cell size measurements in wildtype
853 (*ROR*) and $dPIP4K^{29}$ backgrounds as indicated upon - **D.** Overexpression of insulin receptor (InR)
854 **E.** Overexpression of insulin receptor substrate - Chico **F.** Overexpression of $PDK1^{A467V}$ **G.** Table
855 with differences in median values of cell sizes across different genetic manipulations. Numbers inside
856 the parentheses below the plots indicate the no. of biological replicates used for the measurement.
857 *Mann Whitney test* used for statistical analysis of the distributions. ***p-value* <0.01, ****p-value*
858 <0.001. Genotypes: **B, C.** *AB1Gal4/+ and AB1Gal4; UAS-dINR^{RNAi}*. **D(i).** *AB1Gal4/+ and UAS-*
859 *dINR/+; AB1Gal4/+* and **(ii).** *AB1Gal4/+; $dPIP4K^{29}$ and UAS-dINR/+; AB1Gal4/+; $dPIP4K^{29}$*. **E(i).**
860 *AB1Gal4/+ and UAS-Chico/+; AB1Gal4/+* and **(ii).** *AB1Gal4/+; $dPIP4K^{29}$ and UAS-Chico/+;*
861 *AB1Gal4/+; $dPIP4K^{29}$*. **F(i).** *AB1Gal4/+ and UAS-PDK^{A467V}/+; AB1Gal4/+* and **(ii).** *AB1Gal4/+;*
862 *$dPIP4K^{29}$ and UAS-PDK^{A467V}/+; AB1Gal4/+; $dPIP4K^{29}$*.

863

864 **Fig. 2. Plasma membrane PIP_3 levels are elevated in *dPIP4K* mutant tissues without an increase in**
865 **humoral dILP secretion**

866 **A-B.** PIP_3 quantification – Images showing the intensity and localization of the PIP_3 binding probe
867 (GFP-PH-GRP1) in larval tissues. The PIP_3 levels quantified as the ratio of the probe fluorescence
868 intensity on the plasma membrane to that in the cytosol. **A(i).** Representative confocal images
869 showing the distribution of the probe in the salivary glands. **A(ii).** Quantification of PIP_3 levels
870 between control and $dPIP4K^{29}$ salivary glands for experiment depicted in A(i). (Mean fluorescence
871 intensity ratios calculated from a minimum of 10 cells from each salivary gland). **B(i).** Representative

bioRxiv preprint doi: https://doi.org/10.1101/333153; this version posted June 25, 2018. The copyright holder for this preprint (which was not certified by peer review) is the author/funder, who has granted bioRxiv a license to display the preprint in perpetuity. It is made available under aCC-BY-NC-ND 4.0 International license.

872 confocal images showing the distribution of the probe in the fat body and in **B(ii)** the quantification
873 from these experiments. The ratio was calculated from about 50 cells from 12 fat body regions pooled
874 from 5 animals for each genotype respectively. Wandering third instar larvae used for
875 measurements. Scale: 50 µm for salivary gland images and 10 µm for fat body images **C.** qPCR
876 measurements for mRNA levels of *dILP 2, 3* and *5* from whole larvae. Transcript levels for each gene
877 were normalized to the mRNA levels of *rp49* in the same sample. **D.** qPCR measurements for *dInR*.
878 Transcript levels for each gene were normalized to the mRNA levels of *rp49* in the same sample **E(i).**
879 Confocal z-projections showing immunostaining for dILP2 in larval IPCs, Scale: 50 µm. **E(ii).**
880 Quantification of dILP2 staining intensity in the third instar wandering larval brains. Whiskers in
881 the box plots represent minimum and maximum values, with a line at the median. Numbers inside
882 the parentheses below the plots indicate the no. of biological replicates used for the measurement.
883 *Mann Whitney test* used for statistical analysis of the distributions. **p-value* < 0.05, ***p-value* <0.01.
884 Genotypes: **A-D.** *tGPH and tGPH; dPIP4K*^{29}. **E.** *ROR and dPIP4K*^{29}.
885
886 **Fig. 3. Increased sensitivity of *Drosophila* larval cells to insulin upon loss of dPIP4K.**
887 **A(i).** Confocal z-projections showing levels and localization of the PIP_3 probe in control and
888 *dPIP4K*^{29} in salivary glands cells stimulated with 10 µM insulin for 10 min and in **A(ii),** quantification
889 of PIP_3 levels between control and *dPIP4K*^{29} salivary glands from the same set of experiments.
890 Immunoblot (from wandering third instar stage) showing a reduction in levels of dPIP4K protein in
891 salivary gland lysates upon knockdown of dPIP4K using *AB1*GAL4. **B(ii).** Relative quantification of
892 PIP_3 levels using the GFP-PH-GRP1 probe between control and *dPIP4K*-knockdown salivary glands
893 **C(i).** Confocal z-projections of fat body lobes expressing PIP_3 binding probe from control and
894 *dPIP4K*^{29} late third instar larvae stimulated with 0.1 µM, 1 µM and 10 µM insulin post 2 hr starvation.
895 **C(ii).** Quantification of PIP_3 for experiments in fig. **C** (50 cells from at least 3 samples in the fat body
896 for each genotype and treatment used for analysis). Scale: 50 µm. **C(iii).** Comparison of mean fold

bioRxiv preprint doi: https://doi.org/10.1101/333153; this version posted June 25, 2018. The copyright holder for this preprint (which was not certified by peer review) is the author/funder, who has granted bioRxiv a license to display the preprint in perpetuity. It is made available under aCC-BY-NC-ND 4.0 International license.

change (mutant w.r.t control) in response to insulin computed from data in **B(ii)**. Comparison of PIP_3 levels between (**D**) mutant and rescue salivary glands and (**E**) wildtype and salivary glands overexpressing dPIP4K. Whiskers in the box plots represent minimum and maximum values, with a line at the median. Numbers inside the parentheses below the plots indicate the no. of biological replicates used for the measurement. Scale: 50 µM. *Mann Whitney test* used for statistical analysis of the distributions. **p-value* <0.05, ***p-value* <0.01, ****p-value* <0.001 Genotypes: **A, C.** *tGPH and tGPH; dPIP4K*^{29}. **B.** *AB1Gal4, tGPH/+* **and** *dPIP4K*^{RNAi}*/+; AB1Gal4, tGPH/+*. **D.** *AB1Gal4, tGPH/+; dPIP4K*^{29} and *UAS-dPIP4K/+; AB1Gal4, tGPH/+; dPIP4K*^{29}. **E.** *AB1Gal4, tGPH/+* and *UAS-dPIP4K/+; AB1Gal4, tGPH/+*.

Fig. 4. Quantitative biochemical measurements of PIP_3 identify dPIP4K as a negative regulator of insulin signalling.

A. Schematic outline of the steps involved in LCMS-based measurement of PIP_3 lipid from larvae and cells upon insulin stimulation. **B(i).** Measurement of total PIP_3 levels in whole larval lipid extracts from wildtype (*ROR*) and *dPIP4K*^{29} using LCMS. **B(ii).** Levels of various larval PIP_3 species in wildtype (*ROR*) and *dPIP4K*^{29} whole larval lipid extracts. **C(i).** Measurement of total PIP_3 levels using LCMS in whole cell lipid extracts from S2R+ cells treated with indicated dsRNAs. **C(ii).** Levels of various larval PIP_3 species in whole cell lipid extracts from S2R+ cells. The graphs show mean PIP_3 levels (normalized to spiked internal standards and total organic lipid phosphates recovered). Error bars depict SD. **Inset C(ii).** Immunoblot showing the knockdown of dPIP4K in S2R+ cells using two different sets of dsRNAs. *Student's unpaired t-test* used for statistical analysis of the distributions. **p-value* < 0.05. On each graph, numbers inside the parentheses indicate the no. of biological replicates used for the measurement.

bioRxiv preprint doi: https://doi.org/10.1101/333153; this version posted June 25, 2018. The copyright holder for this preprint (which was not certified by peer review) is the author/funder, who has granted bioRxiv a license to display the preprint in perpetuity. It is made available under aCC-BY-NC-ND 4.0 International license.

Fig. 5. dPIP4K additionally regulates insulin signalling independent of TORC1-mediated negative feedback.

Scheme 1 and **2** depict the feedback regulation of insulin signalling by TORC1 activity in **OFF** and **ON** state respectively. The font and arrow sizes are indicative of the extent of molecular activity. **A-F.** PIP_3 quantification – Salivary gland images showing the distribution of the PIP_3 binding probe GFP-PH-GRP1 in cells. The distribution was quantified as the ratio of probe fluorescence on the plasma membrane to that in the cytosol. In all these experiments, the genetic manipulation was restricted to the salivary glands using *AB1*Gal4. **A, C, E.** In a wildtype background, Downregulation of TOR signalling by RNAi for *Rheb* [**A (i and ii)**]. Upregulation of TOR signalling through overexpression of *Rheb* [**C (i and ii)**], knockdown of *Tsc* [**E (i and ii)**] **B, D, F.** In a *dPIP4K*^{29} background, Downregulation of TOR signalling by RNAi for *Rheb* [**B (i and ii)**] Upregulation of TOR signalling through overexpression of Rheb [**D (i and ii)**], knockdown of Tsc [**F (i and ii)**]. Scale: 50 µM. Whiskers in the box plots represent minimum and maximum values, with a line at the median. Numbers inside the parentheses below the plots indicate the no. of biological replicates used for the measurement. *Mann Whitney test* used for statistical analysis of the distributions. **p-value* < 0.05. ***p-value* <0.01. Genotypes: **A.** *AB1Gal4, tGPH/+ and AB1Gal4, tGPH/ UAS-Rheb*^{RNAi}. **B.** *AB1Gal4, tGPH /+; dPIP4K*^{29} *and AB1Gal4, tGPH/ UAS-Rheb*^{RNAi}*; dPIP4K*^{29}. **C.** *AB1Gal4, tGPH /+ and UAS-dRheb/+; AB1Gal4, tGPH/+*. **D.** *AB1Gal4, tGPH /+; dPIP4K*^{29} *and UAS-dRheb/+; AB1Gal4, tGPH/+; dPIP4K*^{29}. **E.** *AB1Gal4, tGPH /+ and UAS-Tsc1*^{RNAi}*/+; AB1Gal4, tGPH/+*. **F.** *AB1Gal4, tGPH /+; dPIP4K*^{29} *and UAS-Tsc1*^{RNAi}*/+; AB1Gal4, tGPH/+; dPIP4K*^{29}.

Fig. 6. PIP4K functions at the plasma membrane as a negative regulator of insulin receptor signalling

A. Schematic showing constructs that target dPIP4K to different subcellular compartments and the motifs used for targeting. **B (i-iv).** Representative confocal z-projections of S2R+ cells with act-GAL4

bioRxiv preprint doi: https://doi.org/10.1101/333153; this version posted June 25, 2018. The copyright holder for this preprint (which was not certified by peer review) is the author/funder, who has granted bioRxiv a license to display the preprint in perpetuity. It is made available under aCC-BY-NC-ND 4.0 International license.

946 expressing various dPIP4K constructs (**i**) wildtype GFP-tagged dPIP4K (**ii**) plasma-membrane (PM)
947 targeted mCherry-tagged dPIP4K (**iii**) mCherry tagged dPIP4K targeted to various intracellular
948 membranes inclusive of ER, Golgi and endo-lysosomal system (**iv**) GFP-tagged dPIP4K targeted to
949 the lysosome. **C(i).** Immunoblots from S2R+ lysates showing the expression of indicated dPIP4K
950 constructs that were used in the *in vitro* assay. **C(ii).** *In vitro* kinase assay from S2R+ cell lysates
951 showing the activity of different overexpressed dPIP4K constructs. PIP_3 measurement on insulin
952 stimulation (10 μM) using the PH-GFP-GRP1 probe **D-F.** in *dPIP4K*^{29} salivary glands reconstituted
953 with **D.** PM targeted dPIP4K, **E.** endo-membrane targeted dPIP4K, **F.** Lysosomal dPIP4K, **G.** upon
954 overexpression of dPIP4K::mCherry^{CAAX} in the salivary glands. Whiskers in the box plots represent
955 minimum and maximum values, with a line at the median. Numbers inside the parentheses below
956 the plots indicate the no. of biological replicates used for the measurement. *Mann Whitney test* used
957 for statistical analysis of the distributions. **p-value* < 0.05. ***p-value* <0.01. **H(i).** Representative
958 confocal z-projections of CHO-IR cells overexpressing GFP-PIP4K2B and PIP4K2B::mCherry-
959 CAAX. **H(ii).** Immunoblots from CHO-IR cells expressing PIP4K2B constructs stimulated with 1
960 μM insulin for 10 min. The values below the blots represent the mean pAKT/Total AKT ratio across
961 three independent experiments. Genotypes: **D.** *AB1Gal4, tGPH /+ and AB1Gal4, tGPH /+; dPIP4K*^{29}
962 *and AB1Gal4, tGPH /dPIP4K::mCherryCAAX; dPIP4K*^{29}. **E.** *AB1Gal4, tGPH /+ and AB1Gal4, tGPH*
963 */+; dPIP4K*^{29} *and AB1Gal4, tGPH /dPIP4K::mCherryEM; dPIP4K*^{29}. **F.** *AB1Gal4, tGPH /+ and*
964 *AB1Gal4, tGPH /+; dPIP4K*^{29} *and AB1Gal4, tGPH /Lysosomal-dPIP4K::eGFP; dPIP4K*^{29}.
965
966 **Fig. 7. dPIP4K influences PIP_3 turnover.**
967 (**A(i)**) Schematic of the reactions that determine PIP_3 turnover at the plasma membrane. Insulin
968 stimulates PI3K activation. Wortmannin irreversibly inhibits PI3K activity. (**A(ii)**) Live imaging
969 assay protocol to follow PIP_3 dynamics with three phases as depicted. (**B(i)**) A single trace from live
970 imaging of salivary glands expressing GFP-PH-GRP1 probe showing the changes in the plasma-

bioRxiv preprint doi: https://doi.org/10.1101/333153; this version posted June 25, 2018. The copyright holder for this preprint (which was not certified by peer review) is the author/funder, who has granted bioRxiv a license to display the preprint in perpetuity. It is made available under aCC-BY-NC-ND 4.0 International license.

971 membrane to cytosolic ratio of the probe fluorescence over time. **(B(ii))** Wortmannin addition
972 (400nM) completely blocks insulin (10μM) induced PIP_3 production **(B(iii))** DMSO (vehicle)
973 addition does not reduce PIP_3 levels post-insulin (10μM) stimulation. **(C)** and **(D)** Comparison of
974 average traces of GFP-PH-GRP1 fluorescence ratios from multiple imaging runs of *control*, *dPIP4K*^{29}
975 and *dPIP4K overexpression* salivary glands (N=7 for all genotypes). Error bars indicate SD. The two
976 experiments were performed at different times, hence controls samples were repeated. **(E(i) and (ii))**
977 Curves depict changes in slopes of fluorescence calculated by taking ratios of fluorescence from test
978 genotypes to that in controls. The maximal difference is indicated alongside the graph. Genotypes:
979 **B(i-iii).** *AB1Gal4*, *tGPH*/+. **C.** *AB1Gal4*, *tGPH*/+ and *AB1Gal4*, *tGPH*/+; *dPIP4K*^{29}. **D.** *AB1Gal4*,
980 *tGPH*/+ and *UAS-dPIP4K*/+; *AB1Gal4*, *tGPH*/+.
981
982 **Fig. 8. dPIP4K modulates the acquisition of insulin resistance upon high dietary sugar intake.**
983 **A.** The graph represents the mean percentage of pupariation (After egg laying, AEL) observed over
984 time on indicated diets. Data collected from 3 independent batches of about 15-25 larvae per batch
985 (for *ROR and dPIP4K*^{29}). Error bars indicate SD. **B.** Mean hemolymph trehalose levels measured of
986 hemolymph pooled from 5-8 larvae each per genotype (*ROR and dPIP4K*^{29}). Whiskers in the box
987 plots represent minimum and maximum values, with a line at the median. Numbers inside the
988 parentheses below the plots indicate the no. of biological replicates used for the measurement. *Mann*
989 *Whitney test* used for statistical analysis of the distributions. ***p-value* <0.01. **C.** A model for
990 regulation of PIP_3 levels by dPIP4K upon insulin stimulation. In wild-type cells, insulin-induced
991 activation of the receptor triggers dPIP4K activity. This prevents PI5P elevation at plasma membrane
992 and also initiates events that prevent sustained Class I PI3K activity and PIP_3 production. Eventually,
993 the negative feedback via TORC1 activity also sets in. These events act together and keep PIP_3 levels
994 in check. Upon loss of dPIP4K in cells, PI5P accumulates. Class I PI3K shows has a sustained activity

bioRxiv preprint doi: https://doi.org/10.1101/333153; this version posted June 25, 2018. The copyright holder for this preprint (which was not certified by peer review) is the author/funder, who has granted bioRxiv a license to display the preprint in perpetuity. It is made available under aCC-BY-NC-ND 4.0 International license.

995 resulting increased PIP_3 levels upon insulin stimulation which cannot be completely restored via
996 TORC1-mediated negative feedback.
997
998 **Supplementary Figure Legends:**
999 **Fig. S1. Modulatory effect of dPIP4K on insulin signalling in regulation of cell size**
1000 **A-G.** Representative confocal sections of salivary glands of wandering third instar larvae labelled
1001 with BODIPY FL 488 (green) and TOTO3 (red) to mark the nuclei. Scale: 50 µm. Genotypes: **A.**
1002 *AB1Gal4/+ and AB1Gal4/+; UAS-dINR^{RNAi}*. **B.** *AB1Gal4/+ and UAS-dINR/+; AB1Gal4/+*. **C.**
1003 *AB1Gal4/+; dPIP4K^{29} and UAS-dINR/+; AB1Gal4/+; dPIP4K^{29}*. **D.** *AB1Gal4/+ and UAS-Chico/+;*
1004 *AB1Gal4/+*. **E.** *AB1Gal4/+; dPIP4K^{29} and UAS-Chico/+; AB1Gal4/+; dPIP4K^{29}*. **F.** *AB1Gal4/+ and*
1005 *UAS-PDK^{A467V}/+; AB1Gal4/+*. **G.** *AB1Gal4/+; dPIP4K^{29} and UAS-PDK^{A467V}; AB1Gal4; dPIP4K^{29}*.
1006
1007 **Fig. S2. Standardisation of PIP_3measurement using LCMS**
1008 **A.** Linearity of mass spectrometer response for increasing amounts of PIP_3 standard (17:0,
1009 20:4) injected. Each point on the curve indicates the mean ± SD of three replicate injections.
1010 **B.** Chromatograms showing the elution profiles and retention times for various PIP_3 species
1011 detected from whole larval lipid extracts of wildtype larvae stimulated *ex-vivo* with 100 µM
1012 insulin for 10 min. Note the changing retention times with increase in no. of double bonds
1013 and increase in length of acyl chains. Increase in double bonds for a fixed acyl chain length
1014 results in earlier elution. Increase in length of acyl chain delays elution.
1015
1016 **Fig. S3. Biochemical measurement of PIP_3 from larval extracts using LCMS.**
1017 **A.** Relative abundance of various PIP_3 species in whole larval lipid extracts of wildtype larvae
1018 stimulated *ex-vivo* with 100 µM insulin for 10 min. **B.** An experiment showing changes in

bioRxiv preprint doi: https://doi.org/10.1101/333153; this version posted June 25, 2018. The copyright holder for this preprint (which was not certified by peer review) is the author/funder, who has granted bioRxiv a license to display the preprint in perpetuity. It is made available under aCC-BY-NC-ND 4.0 International license.

the levels of various PIP_3 species upon insulin stimulation (100 μM, 10 min). **C(i).** Immunoblot from whole larval lysates showing reduction in levels of dPIP4K protein upon pan-larval RNAi for dPIP4K (*UAS-dPIP4K^{RNAi}/+; daGAL4/+*). **C(ii).** Total levels of PIP_3 in whole larval control and *dPIP4K^{RNAi}* lipid extracts **C(iii).** Levels of various larval PIP_3 species in whole larval control and *dPIP4K^{RNAi}* lipid extracts. Total PIP_3 levels (**D(i)**) and levels of individual species (**D(ii)**) in GAL4-control (*daGAL4/+*), GAL4-control in *dPIP4K^{29}* background (*daGAL4/+; dPIP4K^{29}*) and pan-larval rescue (*daGAL4/UAS-dPIP4K::eGFP; dPIP4K^{29}*) lipid extracts. The graphs show mean PIP_3 levels (normalized to spiked internal standards and total lipid phosphates recovered). Error bars depict SD. On each panel, numbers inside the parentheses indicate the no. of biological replicates used for the measurement.

Fig. S4. PIP_3 measurement with increasing time of insulin stimulation

A(i). Confocal z-projections of salivary glands expressing GFP-PH-GRP1 in wildtype and *dPIP4K^{29}* backgrounds. Salivary glands dissected from wandering 3 rd instar larvae were stimulated or not with 10 μM bovine insulin for indicated times, fixed and imaged. **A(ii).** Relative PIP_3 levels were measured as a ratio of mean fluorescence intensity at the plasma membrane to that in the cytosol. Whiskers in the box plots represent minimum and maximum values, with a line at the median. Numbers inside the parentheses below the plots indicate the no. of biological replicates used for the measurement. *Mann Whitney test* used for statistical analysis of the distributions. ***p-value* <0.01, ****p-value* < 0.001. Genotypes: *AB1Gal4, tGPH/+* and *AB1Gal4, tGPH/+; dPIP4K^{29}*

bioRxiv preprint doi: https://doi.org/10.1101/333153; this version posted June 25, 2018. The copyright holder for this preprint (which was not certified by peer review) is the author/funder, who has granted bioRxiv a license to display the preprint in perpetuity. It is made available under aCC-BY-NC-ND 4.0 International license.

Fig. S5. TORC1 activity regulates cell size in salivary glands.

Cell size measurements in salivary glands upon (**A**) Knockdown of Rheb (**B**) overexpression of dRheb (**C**) Knockdown of TSC in *wildtype* and *dPIP4K*^{29} backgrounds. Whiskers in the box plots represent minimum and maximum values, with a line at the median. Numbers inside the parentheses below the plots indicate the no. of biological replicates used for the measurement. *Mann Whitney test* used for statistical analysis of the distributions. ***p-value* <0.01, ****p-value* <0.001. Genotypes: **A(i).** *AB1Gal4/+ and AB1Gal4/UAS-Rheb*^{RNAi} and **(ii).** *AB1Gal4/+; dPIP4K*^{29} *and AB1Gal4/UAS-Rheb*^{RNAi}*; dPIP4K*^{29} **B(i).** *AB1Gal4/+ and UAS-dRheb/+;* *AB1Gal4/+* and **(ii).** *AB1Gal4/+; dPIP4K*^{29} *and UAS-dRheb/+; AB1Gal4/+; dPIP4K*^{29}. **C(i).** *AB1Gal4/+ and UAS-Tsc1*^{RNAi}*/+; AB1Gal4/+* and **(ii).** *AB1Gal4/+; dPIP4K*^{29} *and UAS-Tsc1*^{RNAi}*/+; AB1Gal4/+; dPIP4K*^{29}. Controls for A(ii) and C(ii) represent values from the same dataset.

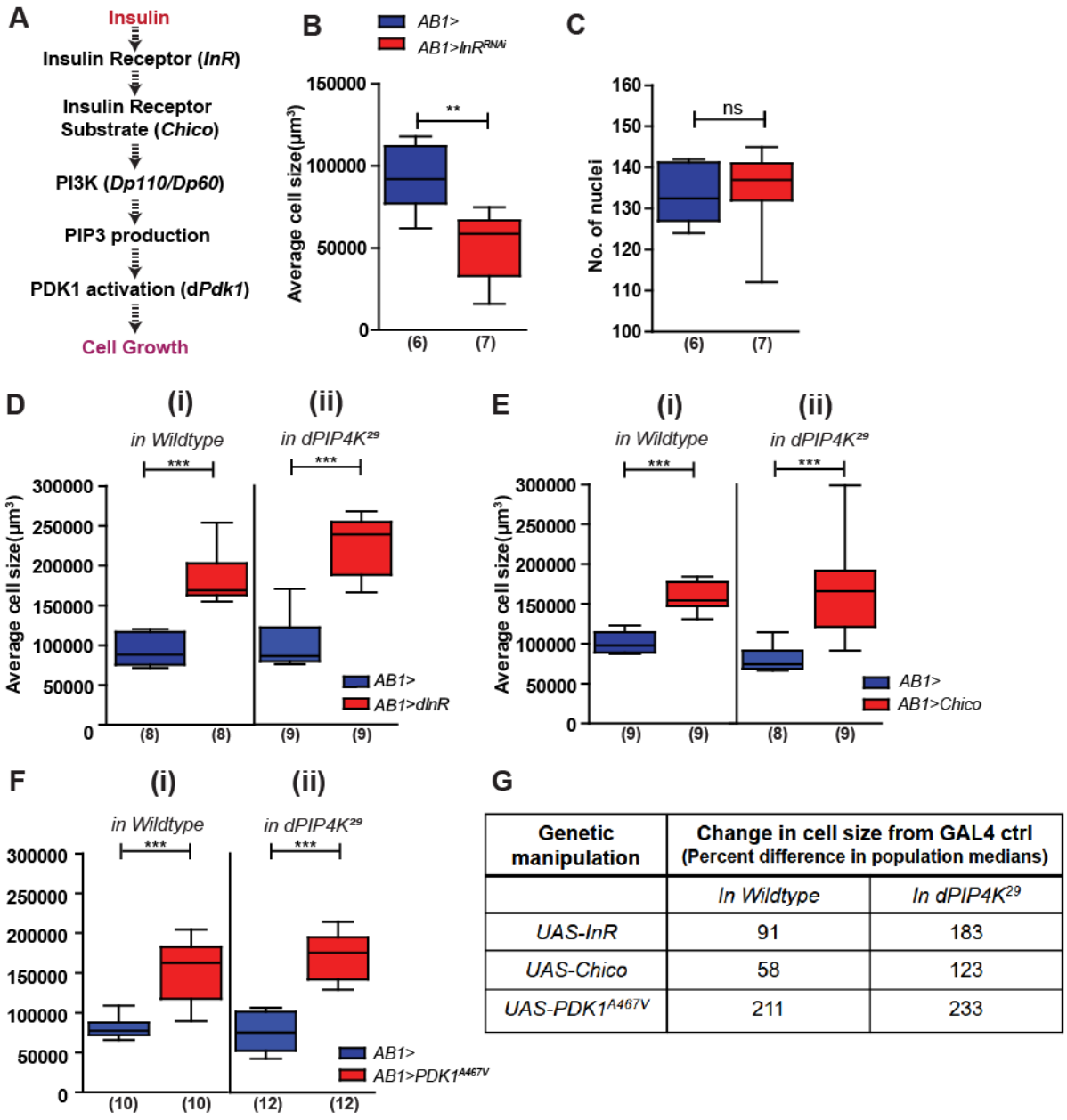

G

Genetic manipulation	Change in cell size from GAL4 ctrl (Percent difference in population medians)	
	In Wildtype	*In dPIP4K²⁹*
UAS-InR	91	183
UAS-Chico	58	123
UAS-PDK1^A467V	211	233

Sharma, et.al. Fig. 1

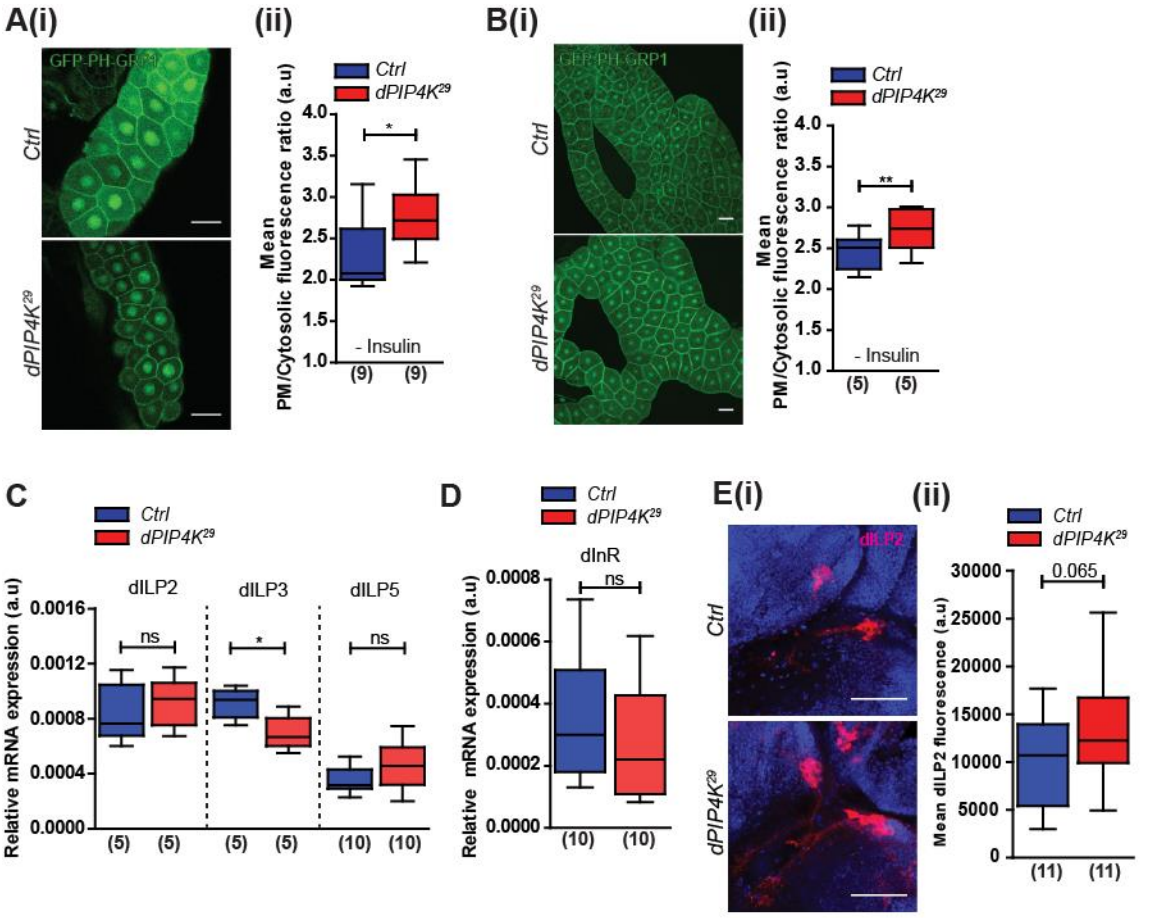

Sharma, et.al. Fig. 2

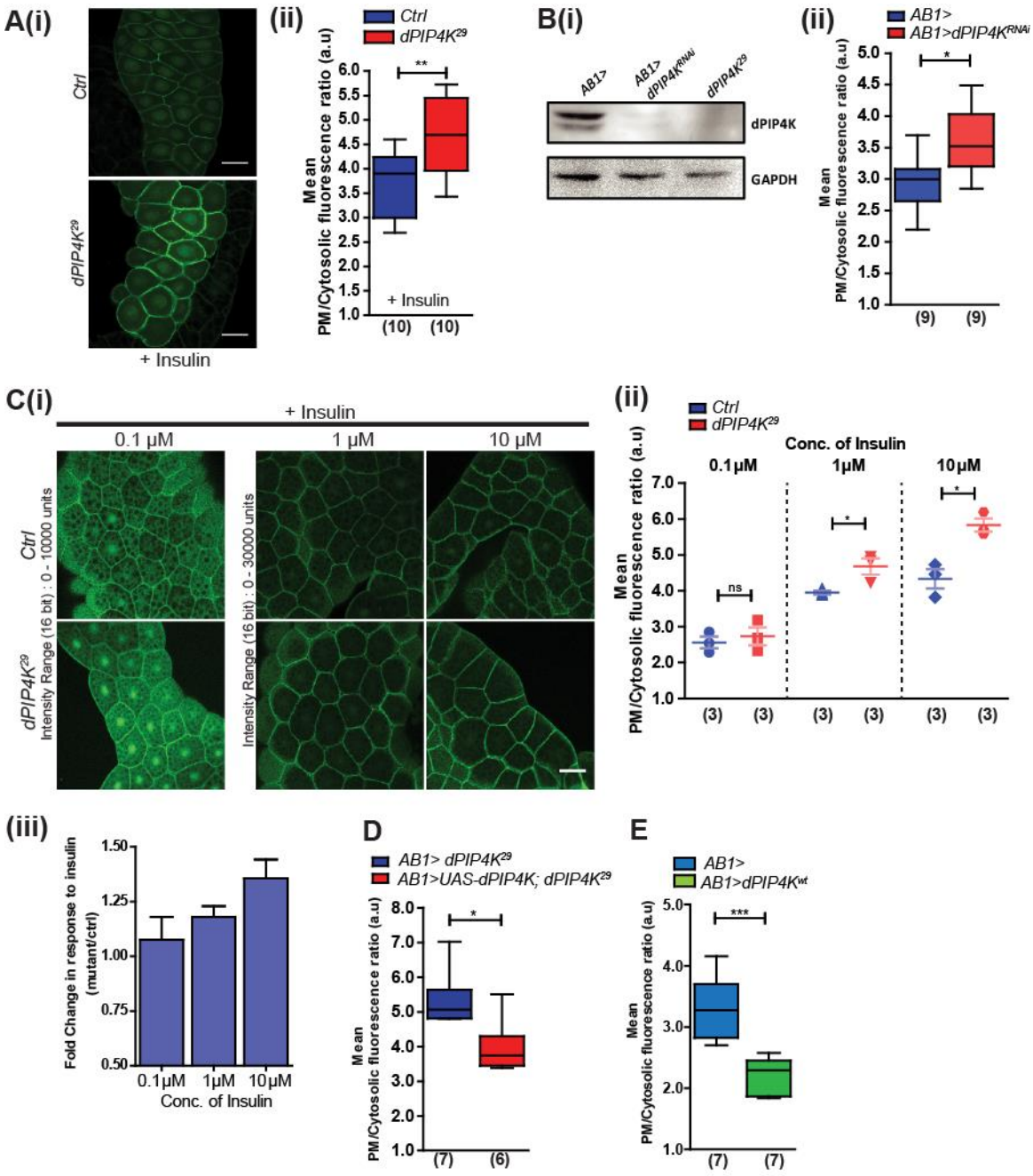

Sharma, et.al. Fig. 3

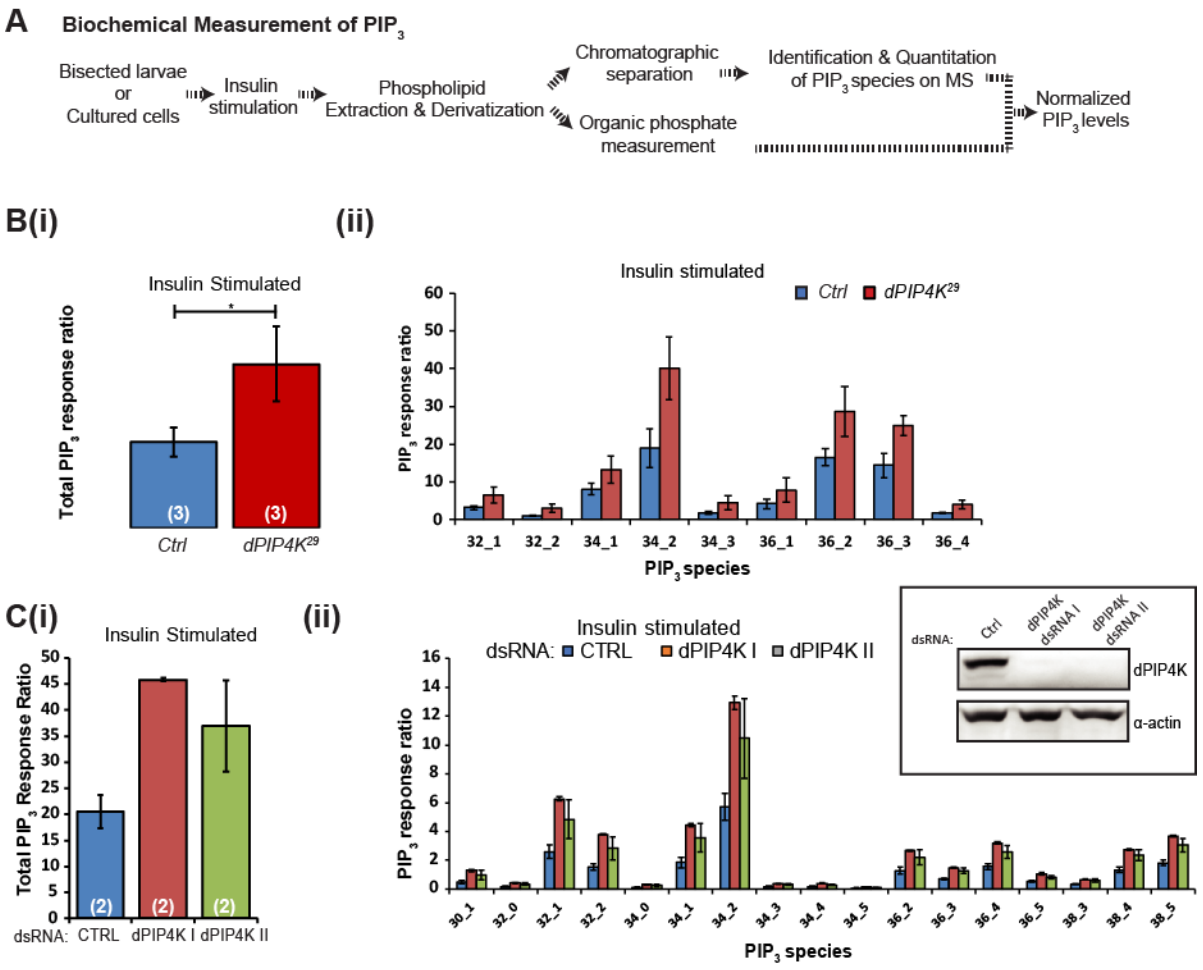

Sharma, et.al. Fig. 4

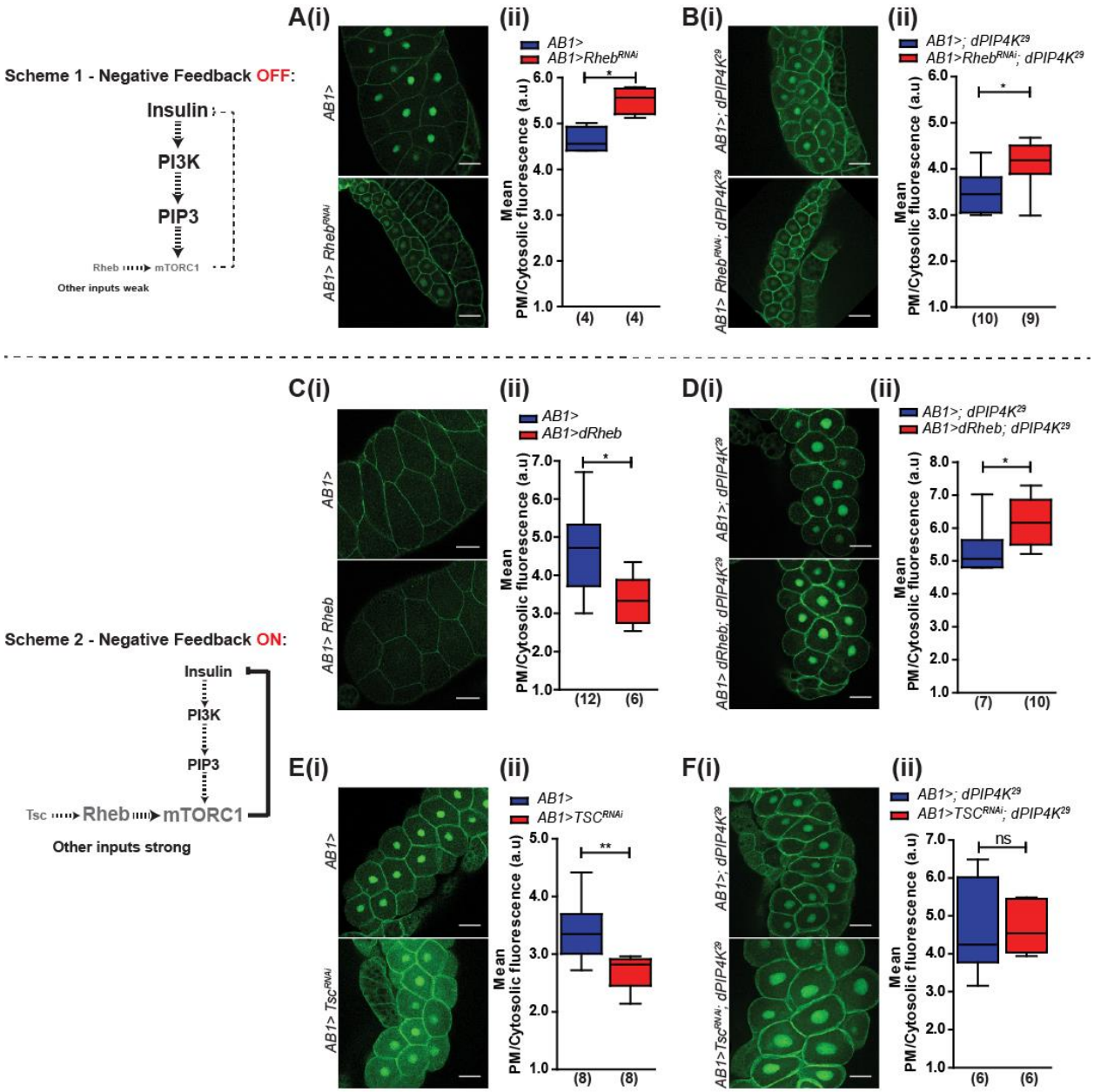

Sharma, et.al. Fig. 5

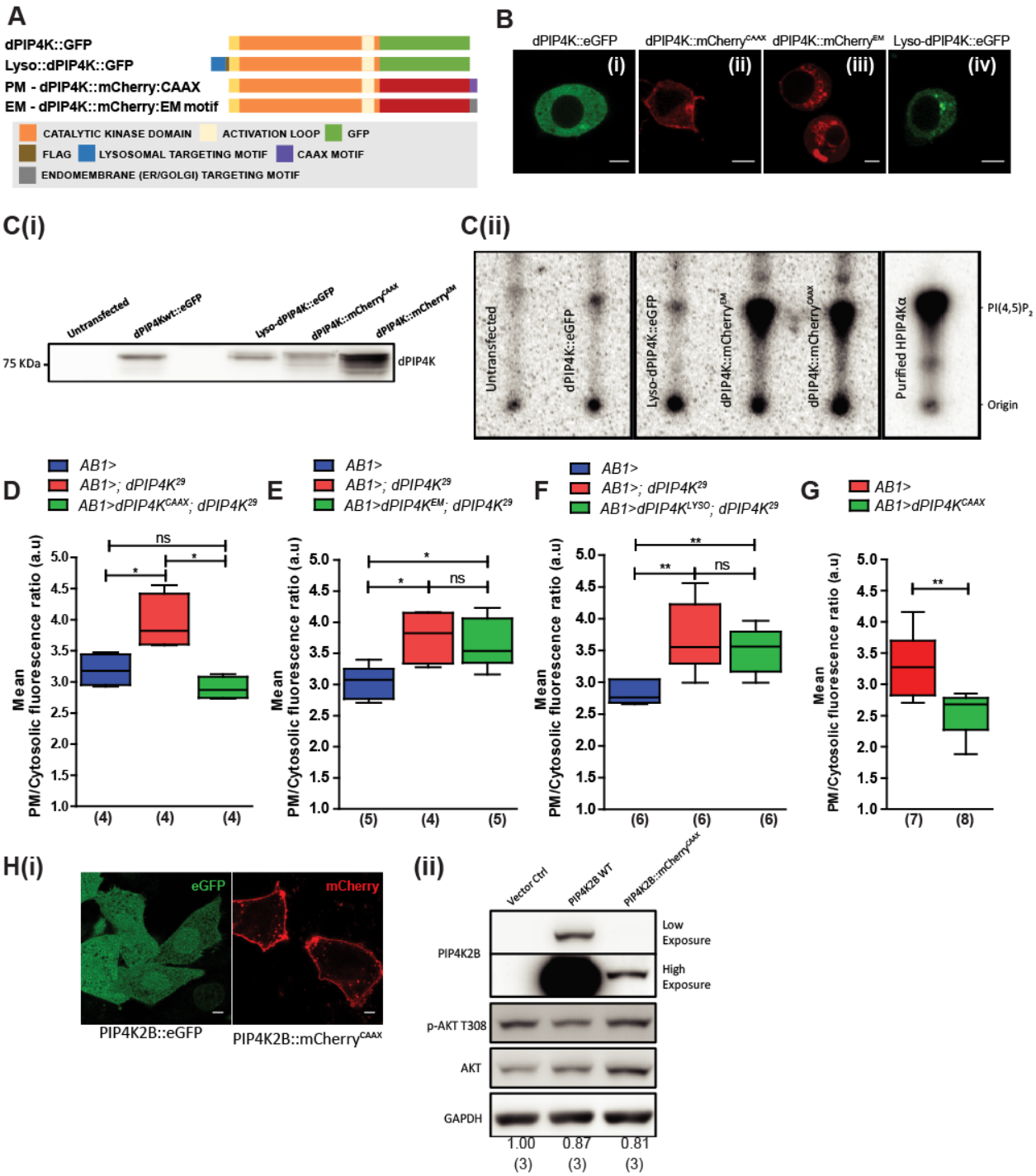

Sharma, et.al. Fig. 6

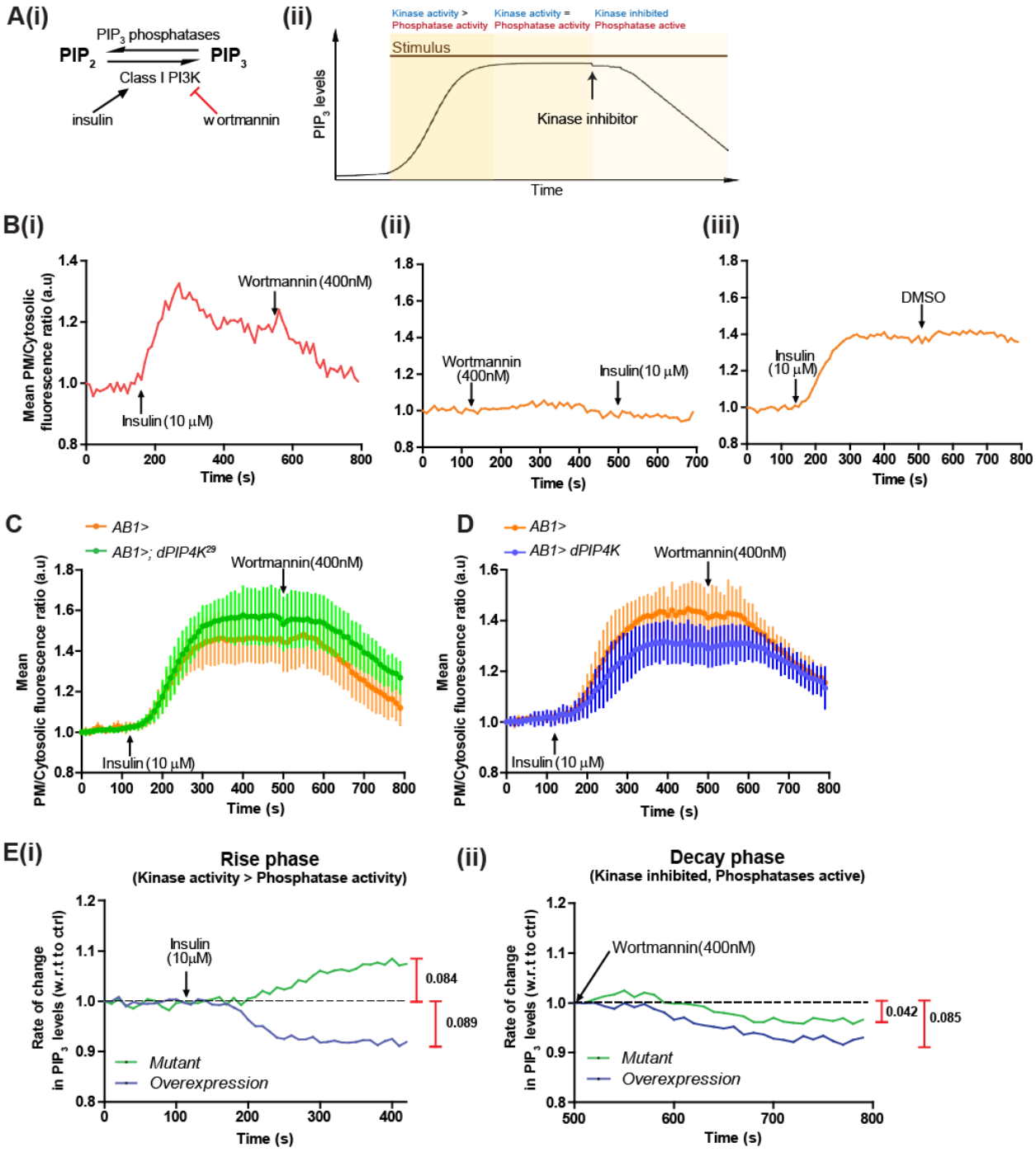

Sharma, et.al. Fig. 7

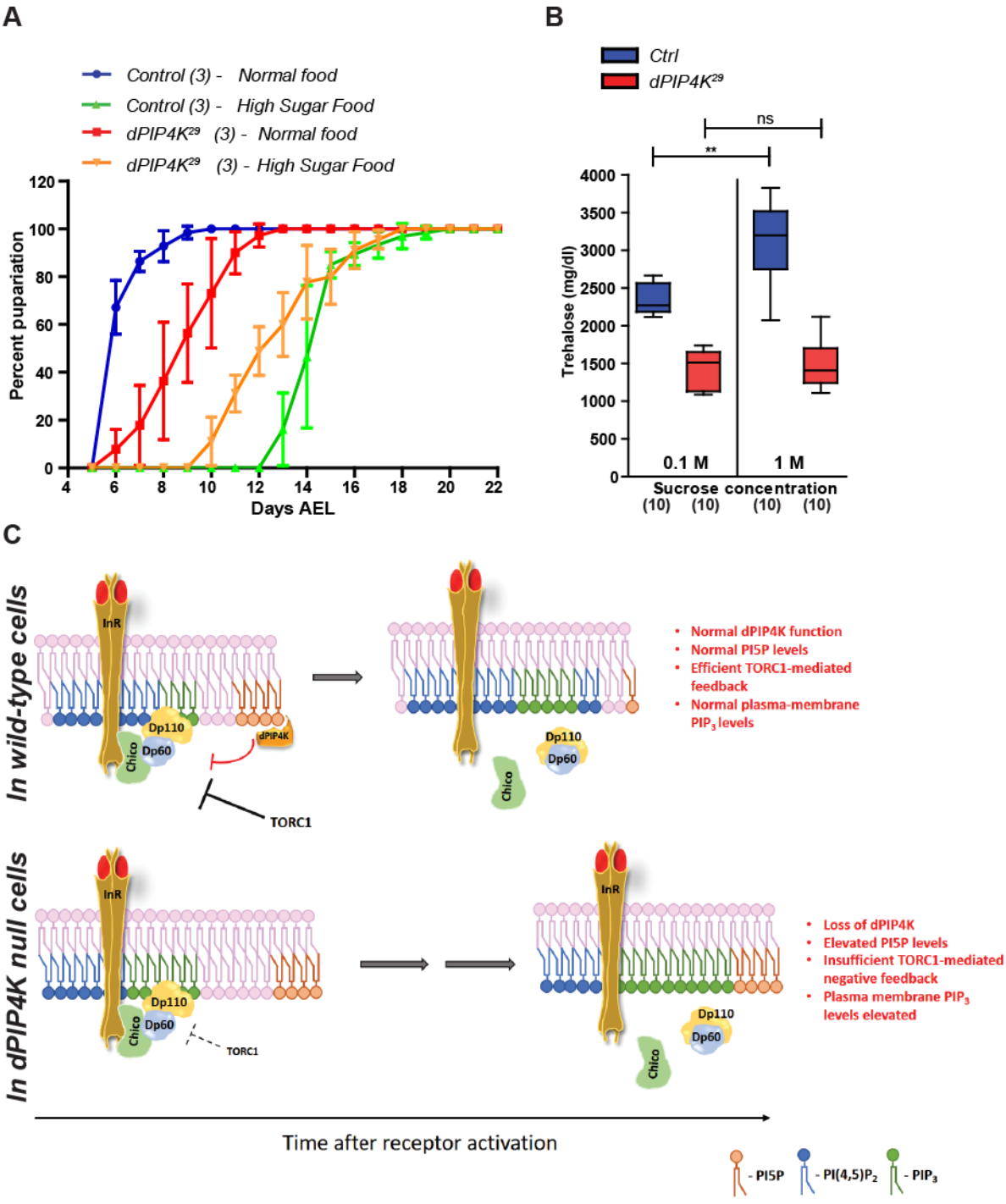

Sharma, et.al. Fig. 8

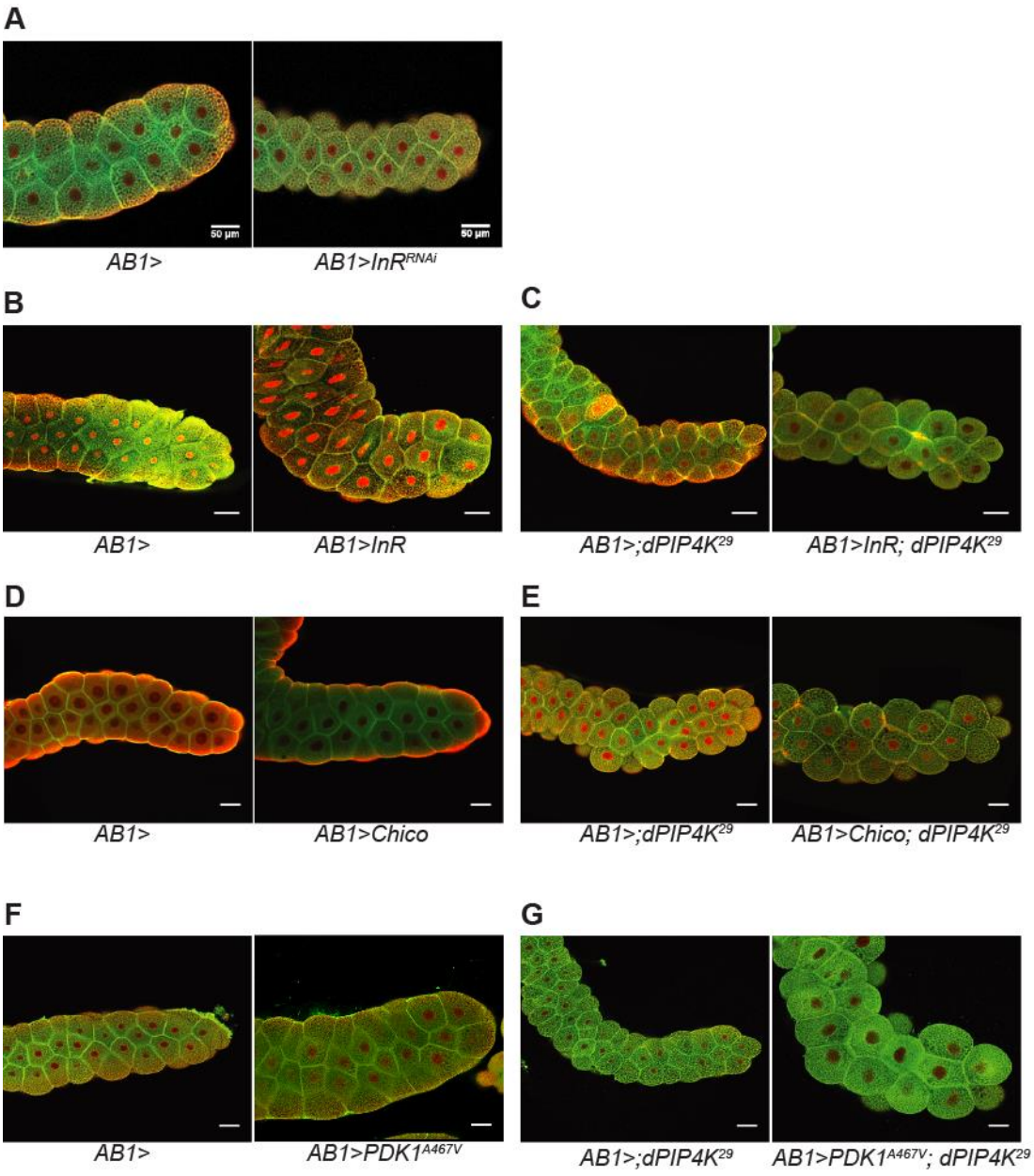

Sharma, et.al. Supplementary Fig. 1 (S1)

A

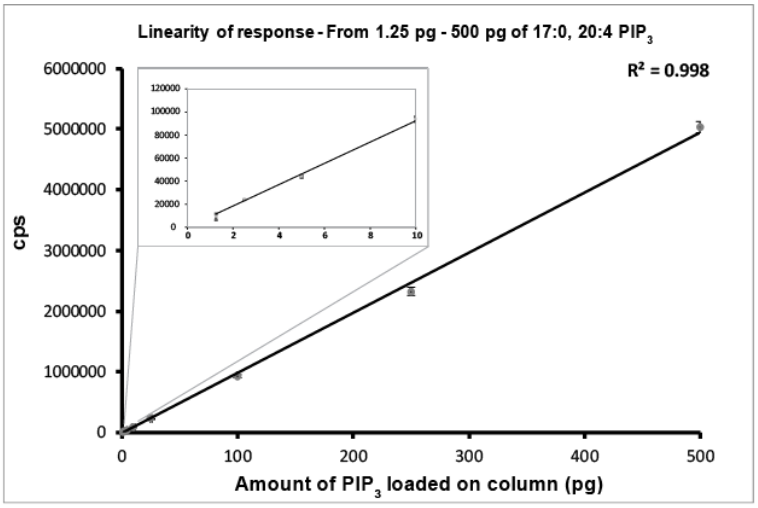

B

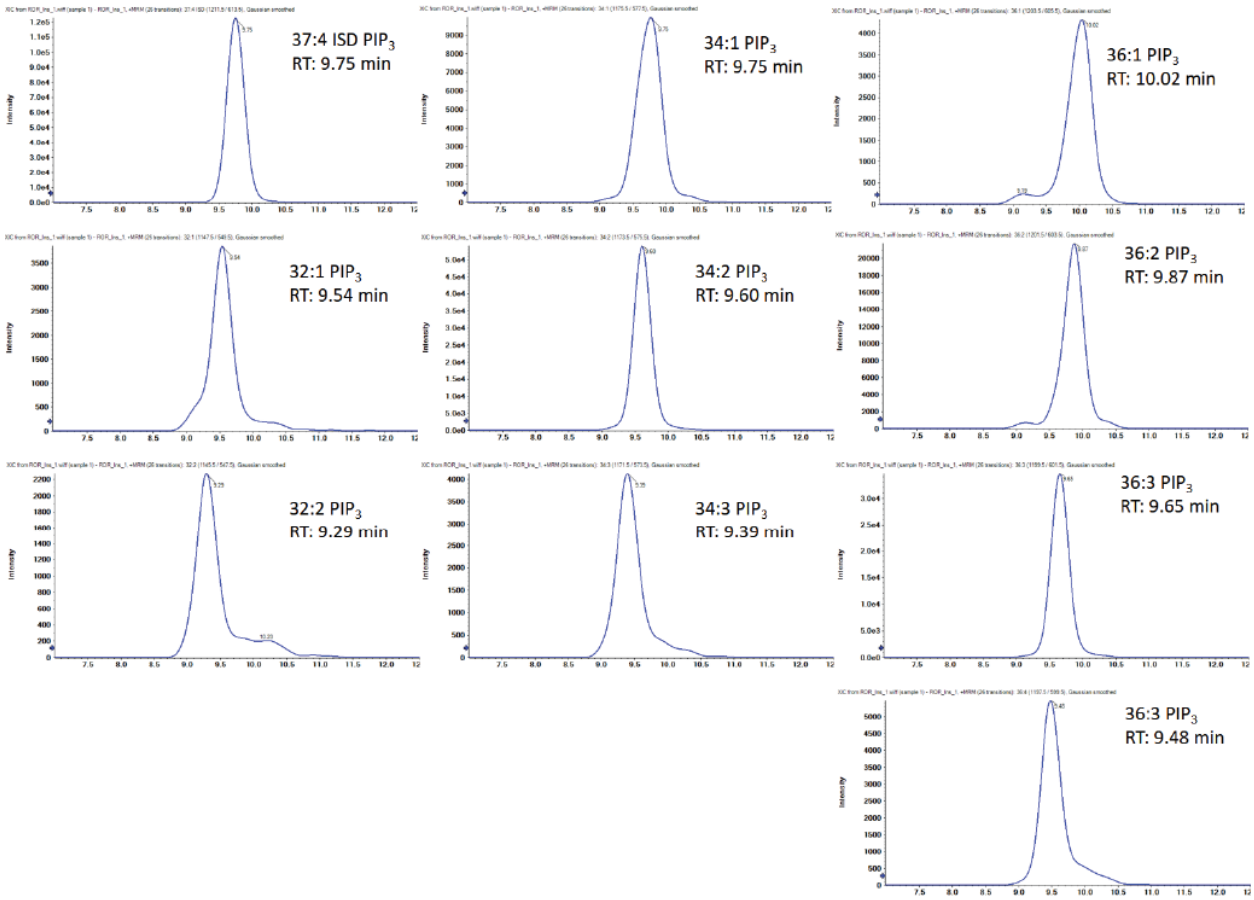

Sharma, et.al., Supplementary Fig. 2 (S2)

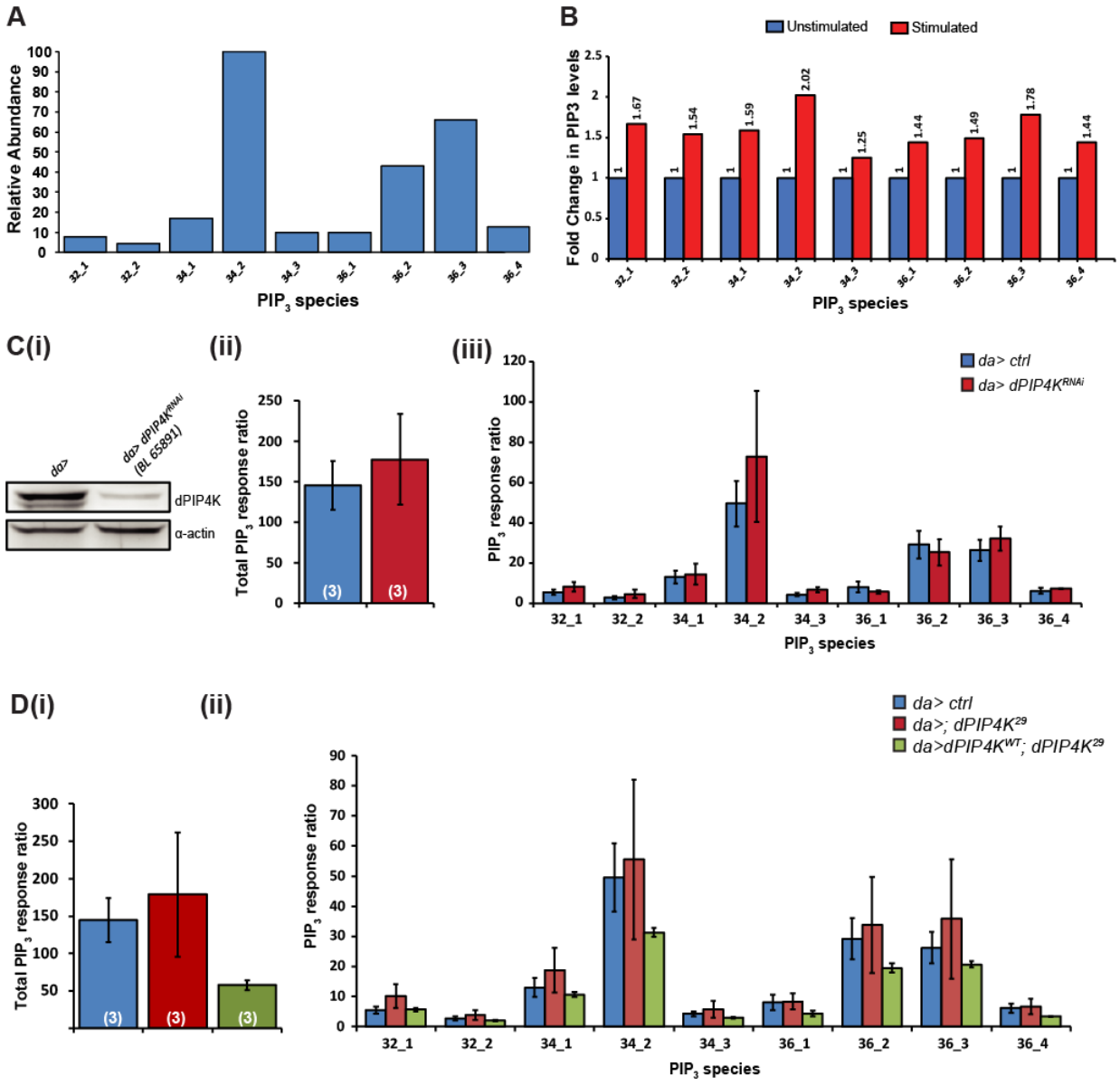

Sharma, et.al., Supplementary Fig.3 (S3)

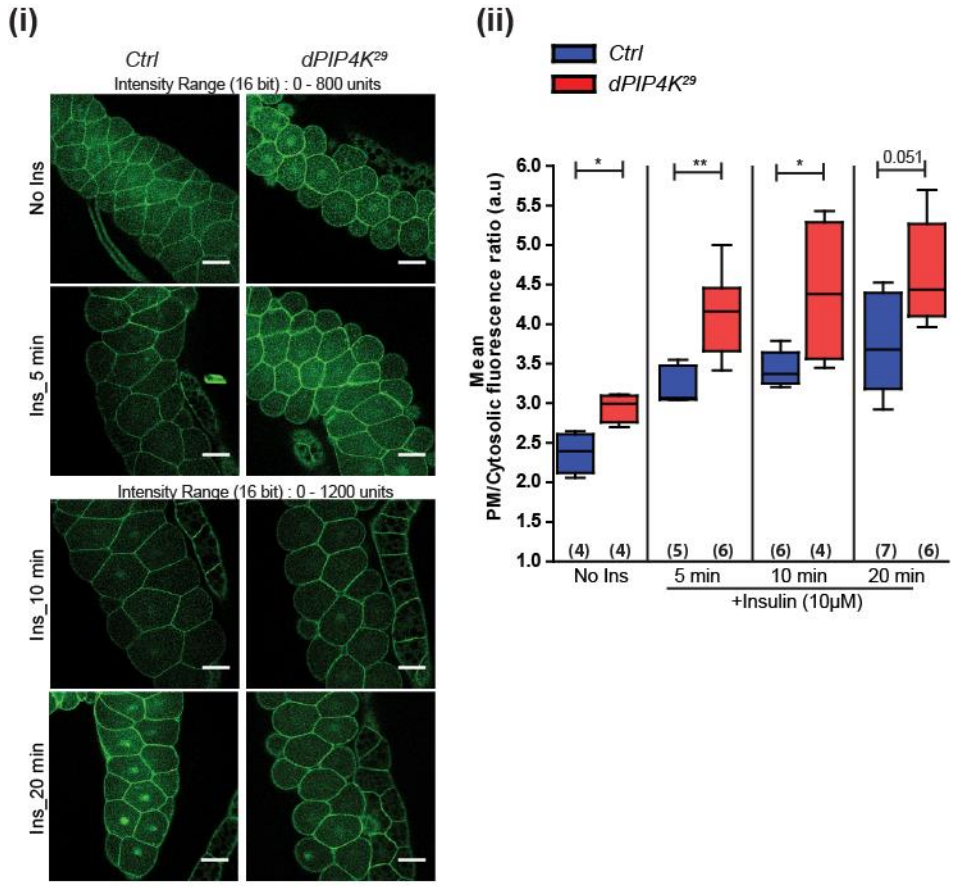

Sharma, et.al., Supplementary Fig. 4 (S4)

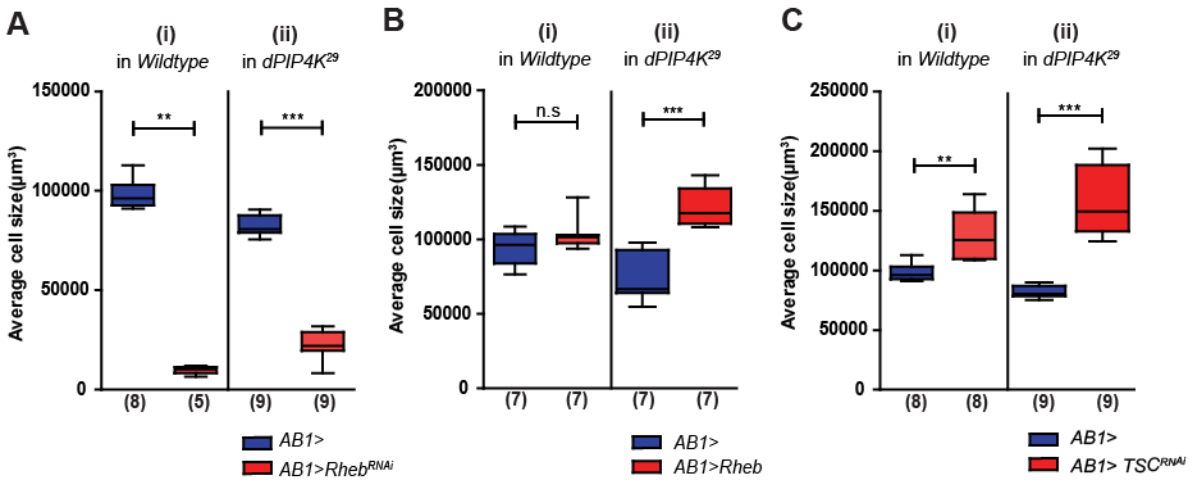

Sharma, et.al. Supplementary Fig. 5 (S5)